

# Multi-Modal Time Series Prediction via Mixture of Modulated Experts

Lige Zhang<sup>1</sup> Ali Maatouk<sup>2</sup> Jialin Chen<sup>2</sup> Leandros Tassiulas<sup>2</sup> Rex Ying<sup>2</sup>

## Abstract

Real-world time series exhibit complex and evolving dynamics, making accurate forecasting extremely challenging. Recent multi-modal forecasting methods leverage textual information such as news reports to improve prediction, but most rely on token-level fusion that mixes temporal patches with language tokens in a shared embedding space. However, such fusion can be ill-suited when high-quality time–text pairs are scarce and when time series exhibit substantial variation in scale and characteristics, thus complicating cross-modal alignment. In parallel, Mixture-of-Experts (MoE) architectures have proven effective for both time series modeling and multi-modal learning, yet many existing MoE-based modality integration methods still depend on token-level fusion. To address this, we propose *Expert Modulation*, a new paradigm for multi-modal time series prediction that conditions both routing and expert computation on textual signals, enabling direct and efficient cross-modal control over expert behavior. Through comprehensive theoretical analysis and experiments, our proposed method demonstrates substantial improvements in multi-modal time series prediction. The current code is available at <https://github.com/BruceZhangReve/MoME>

## 1. Introduction

Time series prediction plays a critical role in a wide range of domains, including energy (Koprinska et al., 2018; Obst et al., 2021), traffic (Alghamdi et al., 2019; Ji et al., 2023), weather (Freeman et al., 2018; Lam et al., 2023), finance (Yin et al., 2021; Ni & Xu, 2023), and many others. Traditional time series models, from statistical approaches such as ARIMA (Zhang, 2003) to deep learning architectures including MLPs (Zeng et al., 2023; Chen

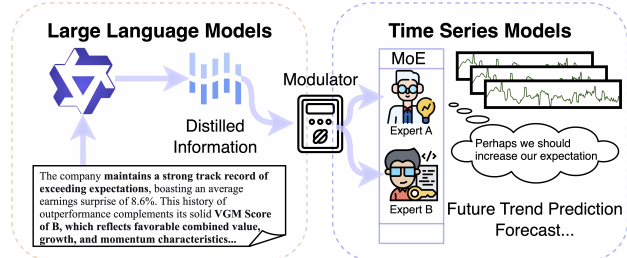


Figure 1. A large language model generates modulation signals that condition both routing and expert computation in a time series MoE model, enabling cross-modal control over temporal experts.

et al., 2023), CNN-based networks (Wu et al., 2023; LIU et al., 2022), RNN-style networks (Rangapuram et al., 2018; Hewamalage et al., 2021), and Transformers (Liu et al., 2022; Zhou et al., 2022; Liu et al., 2024b) have achieved success across different domains. Building on these advances, recent studies (Shi et al., 2025; Liu et al., 2025b) have introduced MoE architectures into time series modeling and achieved promising performance gains.

A common feature of the above methods is that they only use historical sequences for prediction. To that end, they typically struggle when modeling time series in real-world scenarios, such as stock price (Ariyo et al., 2014; Mehtab & Sen, 2020) and air quality (Zaini et al., 2022), where the time series signal alone is often insufficient to fully capture future variations. In practice, external textual information sources, such as news reports, provide additional predictive cues that are not present in the temporal history itself (Wang et al., 2024). This has motivated increasing interest in incorporating auxiliary modalities into time series models, a task referred to as multi-modal time series prediction (MMTSP).

Most MMTSP models are built within a common multi-modal learning framework (Alayrac et al., 2022; Li et al., 2023; Liu et al., 2023): they fuse text tokens and time series tokens (usually temporal patches) in a joint latent space and feed the fused embedding into a pretrained LLM backbone followed by a downstream regression or classification head for prediction (Jin et al., 2024a;b), a paradigm we refer to as **token-level fusion**. Nevertheless, a recent work (Zhang et al., 2025b) systematically evaluated many common fusion strategies and found that MMTSP models built on these schemes do not consistently outperform their uni-modal

<sup>1</sup>Duke Kunshan University, China <sup>2</sup>Yale University, USA. Correspondence to: Rex Ying <rex.ying@yale.edu>.

baselines. This suggests that conventional cross-modal interaction methods do not fully exploit the complementary information in textual signals.

Based on existing studies (Liu et al., 2013; Neubauer & Filzmoser, 2024), we argue that three plausible reasons explain this observation. First, high-quality time-text pairs are limited, and textual counterparts are often noisy or contain substantial information irrelevant to the underlying time signals. Second, textual descriptions can be insufficiently discriminative to capture the subtle differences between similar time series, leading to ambiguous or inaccurate fusion. Third, time series tokens themselves exhibit high heterogeneity: unbounded value ranges, strong non-stationarity, and substantial variation across samples, making the fusion of time and text tokens extremely challenging. These observations call into question the suitability of token-level fusion for MMTSP, raising the question of **whether such an approach can adequately model cross-modal interactions, or whether time series and text demand a different integration mechanism.**

To answer this question, we draw inspiration from real-world decision-making systems, where specialized experts adapt their behaviors in response to auxiliary information beyond historical observations, such as epidemiologists who combine infection trajectories with vaccination reports to make predictions. Motivated by this principle, we propose **Mixture-of-Modulated-Experts** (MoME), a framework that realizes cross-modal interaction via *expert modulation*, in which non-temporal signals directly modulate the computations of temporal experts. Unlike token-level fusion methods that integrate modalities at the representation level, MoME directly injects auxiliary information into expert computations, as shown in Figure 1.

Our main contributions are summarized as follows: (i) we propose *Expert Modulation*, a new paradigm for MMTSP that integrates temporal and textual signals by modulating expert routing and computation within an MoE framework, offering a principled alternative to token-level fusion for multi-modal learning; (ii) we develop a geometric interpretation of MoE and show that sparse routing can be understood as an energy-based truncation mechanism, providing theoretical insight into our modulation design; (iii) we demonstrate the generality and effectiveness of our method across multiple time series backbones, achieving consistent improvements over representative baselines.

## 2. Related Works

**Time Series Prediction via MoE.** MoE (Jacobs et al., 1991) has become a key architectural design in deep learning models (Lepikhin et al., 2021; Fedus et al., 2022), particularly demonstrating strong performance and efficiency in

modern LLMs (DeepSeek-AI et al., 2025; Yang et al., 2025). Recent work has investigated the utilization of MoE in time series models, having successfully developed both small full-shot models (Ni et al., 2024; Sun et al., 2025) and large zero-shot foundation models (Shi et al., 2025; Liu et al., 2025b). However, most studies primarily focus on MoE’s potential for uni-modal time series prediction (UMTSP).

**Multi-Modal Time Series Prediction.** Research in MMTSP has revolved around two main directions: (i) using pre-trained LLMs as expressive sequence encoders (Zhou et al., 2023; Chang et al., 2025; Tan et al., 2024), or (ii) incorporating textual information to aid predictions (Jin et al., 2024a; Jiang et al., 2025). Most existing models rely on token-level fusion (e.g., concatenation or cross-attention) to connect textual and temporal signals (Sun et al., 2024; wang et al., 2025; Quinlan et al., 2026; Zhang et al., 2025b). A separate line of work converts time series into images and applies vision language models for cross-modal learning (Liu et al., 2025a; Zhang et al., 2025a; Shen et al., 2025).

**Multi-Modal Learning via MoE.** mMoE has been widely explored for multi-modal learning (Bao et al., 2022; Shen et al., 2023). A common design allocates separate, modality-specific parameters to different modalities (e.g., modality-specific experts), which has been shown to benefit deep-layer architectures (Wang et al., 2023). More recent approaches introduce modality-aware routing or organize experts into modality-specific pools within each MoE layer (Han et al., 2024; Lin et al., 2024; Lei et al., 2025). However, cross-modal interaction in these methods is still performed at the token (representation) level, whereas our approach operates at the expert (function) level.

## 3. Preliminary

### 3.1. Multi-Modal Time Series

Let  $\mathbf{x} = [x_1, \dots, x_T] \in \mathbb{R}^T$  denote a time series over  $T$  time steps, where  $x_t \in \mathbb{R}$  is the value observed at time  $t$ . In addition to the numerical series, we assume the availability of textual information aligned with the same temporal window. We denote the textual input as a sequence of language tokens,  $\mathbf{s}_{\text{ctxt}} = [s_1, \dots, s_M]$ , representing contextual information (e.g., marketing reports) relevant to the time series, depending on the application domain. The goal of MMTSP is to learn a mapping  $f : (\mathbf{x}, \mathbf{s}_{\text{ctxt}}) \mapsto Y$ , where  $Y$  denotes either (i) a future sequence  $[\hat{x}_{T+1}, \dots, \hat{x}_{T+H}] \in \mathbb{R}^H$  to forecast over a time horizon  $H$ , or (ii) a categorical trend label  $Y \in \{1, \dots, N_c\}$  for trend prediction, where  $N_c$  is the number of trend classes. Unlike conventional time series models that rely solely on numerical sequences, this setting further conditions predictions on the textual descriptions.

### 3.2. Mixture of Experts

An MoE module consists of two main components: a routing network and a set of expert functions. Given a patch size  $L$ , an input sequence is partitioned into  $N$  non-overlapping temporal patches  $\{\mathbf{x}_p\}_{p=1}^N$ , where each patch  $\mathbf{x}_p \in \mathbb{R}^L$  is treated as a token. For each token, the router computes a set of routing scores that determine which experts are activated

$$\mathbf{g}(\mathbf{x}_p) = \sigma(\mathbf{W}_g \mathbf{x}_p) = [g_1(\mathbf{x}_p), \dots, g_E(\mathbf{x}_p)]^\top \in \mathbb{R}^E,$$

where  $E$  is the number of experts,  $\sigma$  is an activation, and  $\mathbf{W}_g \in \mathbb{R}^{E \times d}$  is a trainable projection. Each expert  $f_e(\cdot)$  is a token-wise forward function with a common instantiation

$$f_e(\mathbf{x}_p) = \mathbf{W}_e^{(d)} (\sigma(\mathbf{W}_e^{(u)} \mathbf{x}_p) \odot (\mathbf{W}_e^{(g)} \mathbf{x}_p)),$$

where  $\mathbf{W}_e^{(u)}$ ,  $\mathbf{W}_e^{(g)}$ ,  $\mathbf{W}_e^{(d)}$  denote the up-projection, gating, and down-projection matrices of expert  $e$ , respectively. MoE then combines expert outputs using a Top-K sparse routing

$$\text{MoE}(\mathbf{x}_p) = \sum_{i \in \mathcal{A}} g_i(\mathbf{x}_p) f_i(\mathbf{x}_p) = \sum_{i=1}^E \lambda_i g_i(\mathbf{x}_p) f_i(\mathbf{x}_p),$$

where  $\mathcal{A}$  denotes the index set of selected experts and  $\lambda_i = \mathbb{1}[i \in \text{TopK}(\mathbf{g}(\mathbf{x}_p))]$  is a binary routing mask that satisfies the relationship:  $|\mathcal{A}| = \sum_{i=1}^E \lambda_i = K$ .

## 4. Mixture of Modulated Experts

With the above in mind, we first develop a theoretical interpretation of MoE from a geometric perspective. Building on this view, we introduce our core idea: multi-modal interaction can be achieved by allowing external signals to directly modulate expert behavior within an MoE framework. Then, we present three architectural instantiations of this principle.

### 4.1. MoE from a Geometric Perspective

To formalize a conceptual framework for understanding MoE architectures, we begin by showing that a dense MLP can be decomposed into a sum of smaller sub-MLPs.

**Lemma 4.1** (Decomposition of MLP). *Let  $f(\cdot)$  be a single layer MLP with  $E \times C$  hidden units. Then,  $f(\cdot)$  can be equivalently written as  $f(\mathbf{x}) = \sum_{i=1}^E f_i(\mathbf{x})$ , where each  $f_i(\cdot)$  is a single-layer MLP with  $C$  hidden units, corresponding to a disjoint group of hidden neurons.*

Lemma 4.1, proved in Appendix A.1, holds for common variants of MLP (e.g., FFN or GLU). Under this decomposition, standard MLPs with  $E \times C$  hidden units can be written as a sum of  $E$  sub-MLPs, each containing  $C$  neurons, which can be viewed as a degenerate dense MoE by rewriting the sum as a weighted combination with constant routing coefficients (i.e., for all  $i$ ,  $g_i(\mathbf{x}) = 1$ ). This form suggests that

the MLP output is a superposition of expert contributions  $\{f_i(\mathbf{x})\}_{i=1}^E$ , which we refer to as expert directional signals. A dense MoE can be viewed as an augmentation of this additive structure with a *directional remixing* mechanism

$$\text{MLP}(\mathbf{x}) = \sum_{i=1}^E 1 \cdot f_i(\mathbf{x}) \rightarrow \text{MoE}(\mathbf{x}) = \sum_{i=1}^E g_i(\mathbf{x}) f_i(\mathbf{x}),$$

where the router generates coefficients  $g_i(x)$ , acting as remixing factors, amplifying or attenuating the directional signals produced by different experts.

Sparse routing in MoE further imposes a truncation on this remix via Top-K selection. Geometrically, this corresponds to a truncation that discards directional components with low routing energy (i.e., small  $g_i(\mathbf{x})$ ), analogous to a truncated principal component analysis (PCA) reconstruction where dominant directional components are retained while weaker ones are removed. Beyond computational efficiency, this truncation can potentially act as a denoising step by suppressing low-energy contributions. Theorem 4.2 formalizes this intuition by relating the truncation error to the mass of the discarded coefficient under the coherence assumptions in expert signals.

**Theorem 4.2** (Error Bound of Sparse MoE). *Let  $\{f_i(\mathbf{x})\}_{i=1}^E \subset \mathbb{R}^d$  be the expert directional signals. Assume there exists  $B > 0$  such that  $\|f_i(\mathbf{x})\| \leq B$  for all  $i$ , and  $|\langle f_i(\mathbf{x}), f_j(\mathbf{x}) \rangle| \leq \mu$  for all  $i \neq j$ . Let  $\mathcal{A}$  denote the indices of the  $K$  largest routing coefficients from  $\{g_i(\mathbf{x})\}_{i=1}^E$ . Then, the truncation error*

$$\mathcal{L}(\mathbf{x}) := \left\| \sum_{i=1}^E g_i(\mathbf{x}) f_i(\mathbf{x}) - \sum_{i \in \mathcal{A}} g_i(\mathbf{x}) f_i(\mathbf{x}) \right\|^2,$$

induced by Top-K sparsity, is bounded by

$$\mathcal{L}(\mathbf{x}) \leq [B^2 + (E - K - 1)\mu] \sum_{i \notin \mathcal{A}} g_i(\mathbf{x})^2.$$

Theorem 4.2, proved in Appendix A.2, shows that as  $K$  increases, the upper bound monotonically decreases, allowing the model to retain more directional components; conversely, smaller  $K$  removes more low-energy contributions, producing a smoother (and potentially more denoised) aggregation. This trend is empirically observed: in multiple MoE-based time series forecasting models, sparse activation ( $K < E$ ) shows consistent performance gains over dense activation ( $K = E$ ), as detailed in Appendix B.3.

This interpretation also sheds light on the design of router activation functions. Many previous works instantiate router activation as a SoftMax function (Chen et al., 2022; Jiang et al., 2024), interpreting routing scores as a probability distribution over experts—a choice that can be statistically justified (Nguyen et al., 2024). However, in the energy-based

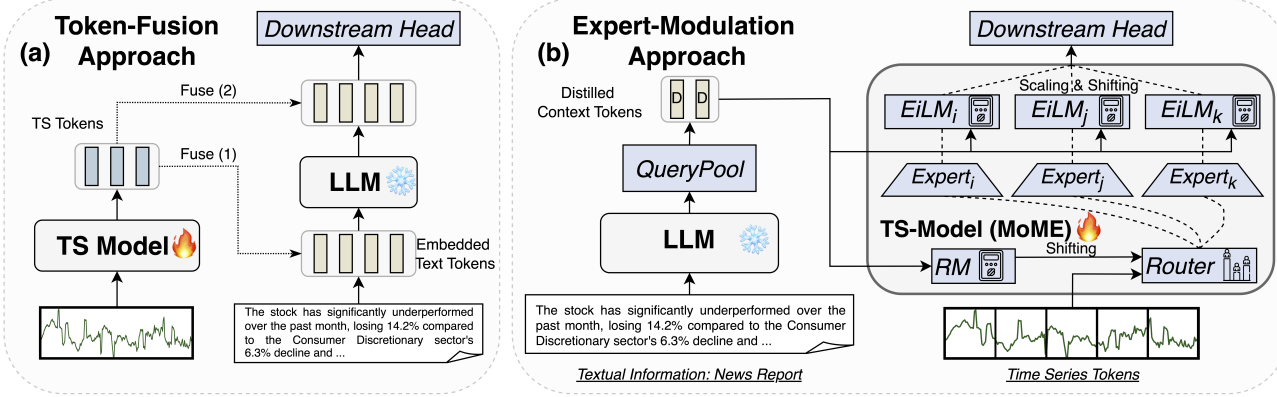


Figure 2. (a): classical Token-level fusion approach, where *Fuse(1)* and *Fuse(2)* denote potential stages that cross-modal fusion to be performed. (b): an instantiation of the proposed *Expert Modulation* multi-modal learning approach. It consists of two main components: *EiLM* (Expert independent Linear Modulation) and *RM* (Router Modulation).

truncation view, routing scores need not form a normalized distribution; instead, they can be understood as unnormalized magnitudes that rescale and remix the energy of an expert direction. In practice, recent work (Han et al., 2024) has already demonstrated such design benefits, which is consistent with our interpretation.

More importantly, this perspective opens a new path for multi-modal integration. If an MoE layer can be understood as a linear remixing of expert directional signals  $\{f_i(\mathbf{x})\}_{i=1}^E$  with input-dependent rescaling coefficients  $\{g_i(\mathbf{x})\}_{i=1}^E$ , then an auxiliary modality can influence the model by **modulating these directional components and/or their remixing weights directly**, rather than relying on token-level fusion or explicit cross-modal alignment. Motivated by this insight, and inspired by conditioning mechanisms in HyperNets (Ha et al., 2017), FiLM (Perez et al., 2018), and controlled GANs (Härkönen et al., 2020), we introduce *Expert Modulation* as a new strategy for multi-modal integration.

#### 4.2. Cross-Modal Interaction via Expert Modulation

*Expert Modulation (EM)* consists of two components: *Expert-independent Linear Modulation (EiLM)* and *Router Modulation (RM)*. EiLM uses textual signals to modulate the outputs of individual temporal experts, whereas RM adjusts the routing scores that determine expert selection. To obtain such textual signals, we extract compact semantic representations from text using a pre-trained LLM, which are then used to modulate routing, and to condition the computations within selected experts. Figure 2 (a) shows the framework of conventional token-level fusion approaches, and Figure 2 (b) demonstrates the expert modulation framework. The three specific steps of EM are described below.

**Step 1: Context Token Distillation.** Given a sequence of language tokens  $\mathbf{s}_{cxt} = [s_1, \dots, s_M]$ , we obtain their

$d$ -dimensional textual representations by applying a linear projection to their final hidden states produced by an LLM

$$\mathbf{H} = \text{LLM}(\mathbf{s}_{cxt}) \mathbf{W}_{proj} \in \mathbb{R}^{M \times d}, \quad (1)$$

where  $\mathbf{W}_{proj} \in \mathbb{R}^{d' \times d}$  such that  $d'$  is the hidden dimension for the LLM. Moreover, we initialize  $m$  trainable and mutually orthogonal query vectors  $\mathbf{Q} \in \mathbb{R}^{m \times d}$  in the latent space. A QueryPool( $\cdot$ ) module then applies cross-attention, using  $\mathbf{Q}$  as queries and  $\mathbf{H}$  as keys and values

$$\mathbf{Z} = \text{SoftMax}\left(\frac{\mathbf{Q} \mathbf{W}_Q (\mathbf{H} \mathbf{W}_K)^\top}{\sqrt{d}}\right) \mathbf{H} \mathbf{W}_V \in \mathbb{R}^{m \times d}, \quad (2)$$

where  $\mathbf{W}_Q, \mathbf{W}_K, \mathbf{W}_V$  denote learnable projection matrices for queries, keys, and values, respectively. This operation produces  $m$  distilled context tokens  $\mathbf{Z}$ , each representing a high-level semantic summary of textual information. These tokens are used to modulate the behaviors of router and experts within MoE-based time series backbone models.

**Step 2: Router Modulation.** We first apply a pooling operator (e.g., average pooling) to aggregate the  $m$  distilled context tokens into a single conditioning vector

$$\mathbf{z} = \text{Pool}(\mathbf{Z}), \quad \text{Pool} : \mathbb{R}^{m \times d} \rightarrow \mathbb{R}^d.$$

Given a patched time series  $\{\mathbf{x}_p\}_{p=1}^N$ , where  $\mathbf{x}_p \in \mathbb{R}^d$ , the router in a time series MoE with  $E$  experts produces an initial routing score  $\mathbf{g}(\mathbf{x}_p) = [g_1(\mathbf{x}_p), \dots, g_E(\mathbf{x}_p)] \in \mathbb{R}^E$ . We then apply a context-to-router mapping to obtain a routing shift from the pooled context tokens

$$\mathbb{G}^{\beta'}(\mathbf{z}) = \mathbf{W}_G \mathbf{z}, \quad \mathbf{W}_G \in \mathbb{R}^{E \times d}.$$

The resulting modulating vector  $\mathbb{G}^{\beta'}(\mathbf{z}) \in \mathbb{R}^E$  then adjusts the original routing scores in a context-dependent manner. Overall, the final routing magnitudes are obtained by

$$\mathbf{g}(\mathbf{x}_p \mid \mathbf{Z}) = \mathbf{g}(\mathbf{x}_p) + \mathbb{G}^{\beta'}(\text{Pool}(\mathbf{Z})). \quad (3)$$

**Step 3: Expert independent Linear Modulation.** For each expert  $f_i(\cdot)$  within the MoE module, we equip it with EiLM modulator functions  $\mathbb{I}_i^\gamma(\cdot)$  and  $\mathbb{I}_i^\beta(\cdot)$ , which generate a context-conditioned scale and bias, respectively

$$\mathbb{I}_i^\gamma(\mathbf{Z}) = \mathbf{w}_i^\top \mathbf{z}, \mathbf{w}_i \in \mathbb{R}^d; \quad \mathbb{I}_i^\beta(\mathbf{Z}) = \mathbf{W}_i \mathbf{z}, \mathbf{W}_i \in \mathbb{R}^{d \times d},$$

where  $\mathbf{z} = \text{Pool}(\mathbf{Z})$  follows the same construction as in Step 2, and  $\mathbf{w}_i, \mathbf{W}_i$  are both trainable weights. We then modulate the  $i$ -th expert output by an affine transformation

$$f_i(\mathbf{x}_p \mid \mathbf{Z}) = \mathbb{I}_i^\gamma(\mathbf{Z}) \cdot f_i(\mathbf{x}_p) + \mathbb{I}_i^\beta(\mathbf{Z}). \quad (4)$$

Finally, we aggregate the modulated experts using the context-conditioned routing scores from the previous step

$$\text{MoME}(\mathbf{x}_p \mid \mathbf{Z}) = \sum_{i=1}^E \lambda_i g_i(\mathbf{x}_p \mid \mathbf{Z}) f_i(\mathbf{x}_p \mid \mathbf{Z}), \quad (5)$$

where the Top- $K$  routing mask  $\lambda_i \in \{0, 1\}$  is defined as

$$\lambda_i = \mathbb{1}[i \in \text{TopK}(\mathbf{g}(\mathbf{x}_p \mid \mathbf{Z}))], \quad \sum_{i=1}^E \lambda_i = K.$$

In this design, contextual signals do not interact directly with temporal tokens. Instead, they enter the MoE by modulating expert behavior through per-expert affine transformations and context-conditioned routing. In contrast, most existing approaches rely on token-level fusion, where temporal tokens are projected and fused with textual tokens in a shared embedding space, as reflected in Figure 2.

### 4.3. Complexity Analysis

Consider a sample with  $N$  temporal tokens and  $m$  distilled context tokens. Let the model dimension be  $d$ , the expert (implemented as FFNs) hidden dimension be  $\tilde{d}$ , the number of experts be  $E$ , and  $K$  experts to be activated per token. Here, we exclude the cost of the pre-trained LLM used for text encoding from the complexity analysis, and primarily focus on the MoE modulation on time series model.

A uni-modal sparse MoE that computes over temporal tokens would introduce computational costs of  $\mathcal{O}(NEd + NKd\tilde{d})$ . Expert modulation introduces two additional sources of overhead: Router Modulation computes a context-conditioned routing shift from pooled context representations at cost  $\mathcal{O}(md + Ed)$ , and EiLM incurs a cost of  $\mathcal{O}(Kdm)$  to generate modulation parameters and  $\mathcal{O}(NKd)$  for element-wise affine modulation of selected experts. Since, in practice,  $\tilde{d} \gg m, E$ , the dominant term remains  $\mathcal{O}(NEd + NKd\tilde{d})$ . Therefore, MoME achieves multi-modal integration without changing the asymptotic complexity of the uni-modal sparse MoE backbone.

### 4.4. Expert Modulation on Different Backbones

Expert Modulation defines a general, backbone-agnostic principle for multi-modal time series modeling. To demonstrate its flexibility, we instantiate this framework in three representative architectures with increasing modeling complexity: a linear model (MMLinear), an MLP-based model (MoME), and a transformer-based model (MiTransformer).

- (i) **MoME** is the primary instantiation of our framework. The input time series is segmented into patches. Experts are implemented as MLPs with expert modulation applied.
- (ii) **MMLinear** is a lightweight variant that operates directly on the full sequence, where each expert is reduced to a linear transformation with expert modulation applied.
- (iii) **MiTransformer** is a multi-modal extension of iTransformer that replaces FFN blocks with MoME modules. It also operates on the full sequence without patching.

## 5. Experiments

We comprehensively evaluate MoME by addressing three core questions. First, we assess whether MoME delivers robust predictive performance across diverse time series domains, temporal horizons, and textual complexities (Q1; Section 5.2). Second, we investigate whether expert-level cross-modal interaction offers advantages over standard token-level fusion mechanisms (Q2; Section 5.3). Finally, we examine the role of textual conditioning in shaping time series prediction behavior (Q3; Section 5.4).

### 5.1. Experiments Setup

**Datasets.** To validate our theoretical insights into MoE (Theorem 4.2), we conduct experiments on seven UMTSP datasets (detailed results in Appendix B.3), including electricity, exchange rates, and traffic (Lai et al., 2018; Zhou et al., 2021; Wu et al., 2021). To test our method for MMTSP, we conduct experiments on weather and finance datasets from MT-Bench (Chen et al., 2025), and on five multi-modal benchmarks spanning environmental, epidemiological and economic domains from TimeMMD (Liu et al., 2024a). Detailed experimental protocols are provided in Appendix C.1 and Appendix C.2.

**Baselines without External Text Inputs.** Under the UMTSP frameworks, we select five state-of-the-art baseline models, including PatchTST (Nie et al., 2023), iTransformer (Liu et al., 2024b), TS-Mixer (Chen et al., 2023), DLinear (Zeng et al., 2023), and TimeMoE (Shi et al., 2025). To further assess the benefits of incorporating language models, we evaluate two LLM-enhanced prediction methods, GPT4TS (Zhou et al., 2023) and Time-LLM (Jin et al., 2024a). We follow a common setting where the language

Task	Metric	PatchTST	DLinear	TS-Mix	Time-MoE	Time-LLM	GPT4TS	Time-MoE +LM	DLinearP +LM	MLP(MoE) +LM	MoME (ours)	Imp. (%)
<b>MTBench: Forecast</b>												
Finance (Short)	MAPE $\downarrow$	2.774	2.863	2.759	3.419	2.898	2.944	2.772	2.805	<b>2.545</b>	<b>2.605</b>	-2.357
	MAE $\downarrow$	3.264	3.383	3.220	3.984	3.411	3.540	3.248	3.419	<b>3.136</b>	<b>3.058</b>	2.487
Finance (Long)	MAPE $\downarrow$	3.832	3.853	3.802	4.564	4.328	4.272	<b>3.749</b>	4.010	3.757	<b>3.531</b>	5.815
	MAE $\downarrow$	3.604	3.620	3.553	4.326	4.023	3.886	<b>3.427</b>	3.606	3.523	<b>3.253</b>	5.077
Weather (Short)	MSE $\downarrow$	10.448	10.438	18.222	21.635	10.658	11.947	<b>10.211</b>	10.374	11.233	<b>10.020</b>	1.871
	MAE $\downarrow$	2.404	2.449	3.292	3.572	2.453	2.537	<b>2.397</b>	2.407	2.508	<b>2.389</b>	0.333
Weather (Long)	MSE $\downarrow$	14.312	13.392	24.445	40.887	<b>12.805</b>	13.901	14.894	13.666	13.331	<b>11.823</b>	7.669
	MAE $\downarrow$	2.857	2.765	3.846	5.010	<b>2.738</b>	2.812	2.923	2.809	2.771	<b>2.620</b>	4.310
<b>MTBench: Trend Predict</b>												
Finance (Short)	3-way $\uparrow$	39.674	38.044	47.826	42.391	40.761	48.913	46.739	<b>49.315</b>	43.478	<b>66.849</b>	17.534
	5-way $\uparrow$	40.217	29.348	<b>42.391</b>	38.044	38.587	40.217	35.326	39.041	40.127	<b>55.978</b>	13.587
Finance (Long)	3-way $\uparrow$	<b>50.802</b>	41.096	50.685	44.178	49.315	48.287	48.630	45.109	48.288	<b>62.671</b>	11.869
	5-way $\uparrow$	41.438	30.822	<b>44.521</b>	36.645	42.123	41.438	30.822	41.848	33.219	<b>51.027</b>	6.506
Weather (Short)	Past $\uparrow$	<b>93.877</b>	69.231	91.484	85.440	87.918	88.189	<b>92.582</b>	89.011	91.758	91.484	-2.393
	Future $\uparrow$	51.374	50.824	53.022	<b>53.571</b>	42.674	53.297	42.307	42.582	43.132	<b>55.220</b>	1.649
Weather (Long)	Past $\uparrow$	89.973	82.656	90.786	89.431	84.553	85.366	<b>91.599</b>	88.347	86.450	<b>93.496</b>	1.897
	Future $\uparrow$	26.558	49.865	48.510	<b>50.949</b>	50.407	42.005	42.276	41.192	<b>52.575</b>	1.626	
<b>TimeMMD: Forecast</b>												
Environment	MAPE $\downarrow$	28.270	28.519	27.682	25.659	26.712	26.563	<b>25.141</b>	25.628	26.886	<b>15.434</b>	38.610
	MAE $\downarrow$	16.331	16.294	16.162	14.947	15.318	15.206	<b>14.925</b>	14.942	15.520	<b>8.317</b>	44.274
Energy	MSE $\downarrow$	0.064	0.031	0.031	0.016	0.016	0.015	<b>0.014</b>	0.015	0.021	<b>0.015</b>	-7.143
	MAE $\downarrow$	0.187	0.120	0.123	0.082	0.087	0.082	<b>0.078</b>	0.079	0.098	<b>0.081</b>	-3.846
Health (US)	MSE $\downarrow$	1.503	0.929	0.867	0.789	0.851	0.824	<b>0.587</b>	0.730	0.802	<b>0.379</b>	35.434
	MAE $\downarrow$	0.832	0.614	0.553	0.483	0.530	0.504	<b>0.445</b>	0.468	0.489	<b>0.359</b>	19.325
Health (AFR)	MSE $\downarrow$	0.239	0.186	0.206	0.152	0.141	<b>0.134</b>	0.197	0.173	0.195	<b>0.103</b>	23.134
	MAE $\downarrow$	3.465	2.970	3.106	2.621	2.567	<b>2.551</b>	2.894	2.682	2.992	<b>2.303</b>	9.722
Social Good	MSE $\downarrow$	2.406	2.116	2.413	<b>1.795</b>	2.020	1.817	2.191	1.929	1.908	<b>1.419</b>	20.947
	MAE $\downarrow$	0.786	0.709	0.654	<b>0.519</b>	0.541	0.496	0.739	0.744	0.730	<b>0.417</b>	15.927

Table 1. The model performance across MTBench and TimeMMD.  $\downarrow$  /  $\uparrow$  indicates lower/higher is better. For Health (AFR), MSE/MAE are reported in units of  $10^2$ . Red bold indicates best; bold indicates second best. Imp. (%) is compared with the strongest baseline.

model is frozen and only the forecasting head is trained.

**Baselines Supporting External Text Inputs.** We implement three MMTSP baselines following the token-level fusion principles summarized in (Zhang et al., 2025b). In the main experiments, we report results for MLP (MoE)+LM, TimeMoE+LM, and DLinearP+LM, where “+LM” means incorporating external text by token-level fusion. Here, MLP (MoE) is a simple MoE network composed of MLP experts, and DLinearP is a DLinear model with patching.

**Settings.** To ensure fair comparison, we standardize key hyperparameters (e.g., hidden dimensions and number of layers) and align training configurations across all experiments. All models are implemented in PyTorch and trained on a single NVIDIA RTX A6000 (48GB) GPU. For text processing, we use a pre-trained LLM (QwenMoE\_A2.7B) and truncate the maximum text length to 2048 tokens. Full experimental details are provided in the Appendix D.6.

## 5.2. Effectiveness for Prediction

We evaluate MoME in two complementary regimes. The first is long-horizon forecasting with complex context, where models observe long histories (e.g.,  $\geq 100$  look-back steps) and predict extended futures (e.g.,  $\geq 25$  steps), paired with lengthy and noisy texts; this setting is evaluated on MTBench. The second is short-horizon forecasting with

a simple context, where both the look-back window (e.g.,  $\leq 20$  steps) and prediction horizon (e.g.,  $\leq 5$  steps) are short, and textual descriptions are concise and closely related to the target series; this setting is evaluated on TimeMMD. The results for both regimes are reported in Table 1.

**Long Horizon Complex Context.** MoME achieves significant improvements over the strongest baselines in both datasets. The gains are most pronounced on the finance (stock price) trend prediction task, indicating that textual information is particularly effective in capturing directional or trend-level signals, rather than precise numerical values. Overall, these results demonstrate that MoME can effectively extract useful information from complex and noisy contexts and benefit long-horizon prediction.

**Short Horizon Simple Context.** MoME achieves the best performance in most settings, with improvements that are often greater than those observed in the long-horizon regime. A plausible explanation is that, while textual reports complement the short-term dynamics, they provide limited information about long-term behaviors. For example, news reports focusing on near-term air quality are often weakly predictive beyond the reported time window. Together, these findings suggest that MoME delivers consistent improvements across various time series prediction tasks, spanning different temporal horizons and levels of textual complexity.

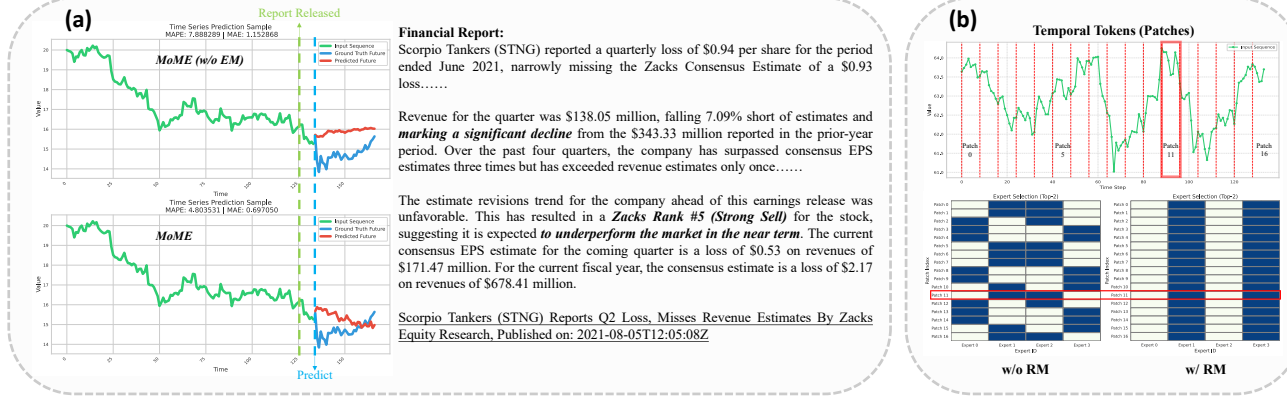


Figure 3. (a): A case study comparison between the *Expert Modulation* (EM) based multi-modal MoME and the uni-modal variant MoME (*w/o* EM). (b): The change in routing behavior when activating router modulation (*w/o* RM).

### 5.3. Comparison with Token-Level Fusion Strategies

We further compare our model with a series of token-fusion based variants. To ensure a fair comparison, we only change the way of injecting multi-modal information while keeping other settings identical. Specifically, we first disable expert modulation to obtain a uni-modal variant, denoted as MoME (*w/o* EM). We then use this model as the backbone and attach different token-level fusion modules, including early and late fusion strategies illustrated in Figure 4 (a), to integrate textual information with time series input at the token level (implementation details are provided in Appendix D.4). We compare these models from multiple perspectives, including predictive performance, memory consumption, and inference speed, with the results summarized in Figure 4 (a). Compared to token-fusion baselines, the proposed expert-modulation method achieves better performance while maintaining favorable efficiency.

### 5.4. The Role of Multi-Modality

To investigate how textual information influences the time series model, we conduct a case study on stock price prediction, presented in Figure 3 (a). The historical price exhibits an overall downward trend, with a noticeable slowdown in the most recent period. As a result, the uni-modal variant, MoME (*w/o* EM), extrapolates the recent pattern and predicts that the future price would remain relatively stable. In contrast, recent financial reports provide strong signals (multiple adverse market factors) indicating a potential further decline in the price. By incorporating these external textual signals, the full MoME model is able to anticipate the impending downward trend more accurately. This results in a substantial accuracy gain, reducing MAPE by nearly 50% relative to uni-modal prediction. Even in cases where the external report contains misleading or incorrect information, MoME maintains comparable performance to its uni-modal variant MoME (*w/o* EM), demonstrating the model's robustness to noisy multi-modal knowledge. We discuss such representative cases in the Appendix E.

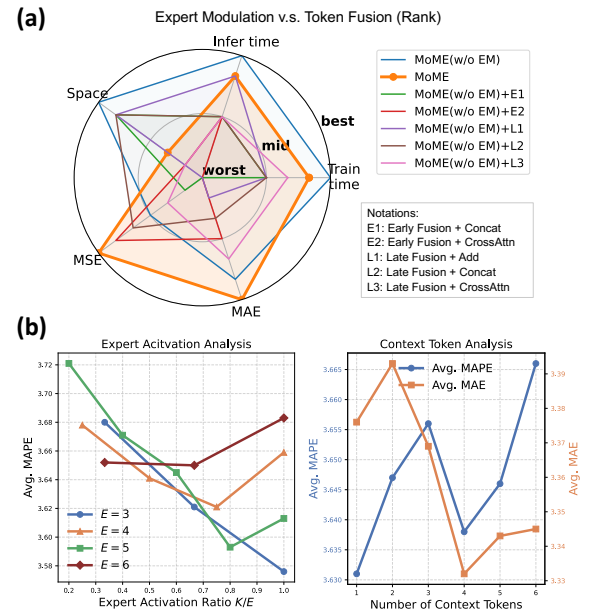


Figure 4. (a): Comparison between token fusion and expert modulation. (b): Comparison on hyperparameter effects.

robustness to noisy multi-modal knowledge. We discuss such representative cases in the Appendix E.

### 5.5. Ablation Studies

**Component Effect.** To assess the effectiveness of Expert Modulation, we conduct component-level ablation studies by removing EiLM or RM from the tested backbones while keeping other hyperparameters identical. In particular, we test three instantiations of the framework, including MoME, MMLinear, and MiTransformer, as described in Section 4.4. The results in Table 2 show that incorporating EiLM consistently improves performance over uni-modal baselines across all backbone families, and introducing RM yields

Task	Metric	MoME			MMLinear			MiTransformer			Avg. Imp. (%)
		w/o EM	w/ EiLM	w/ RM	w/o EM	w/ EiLM	w/ RM	w/o EM	w/ EiLM	w/ RM	
<b>MT-Bench: Forecast</b>											
Finance (Short)	MAPE $\downarrow$	2.670	<b>2.659</b>	2.744	2.856	2.819	<b>2.803</b>	<b>2.775</b>	3.039	3.039	-2.415
Finance (Short)	MAE $\downarrow$	3.207	<b>3.117</b>	3.158	3.392	3.311	<b>3.305</b>	<b>3.234</b>	3.545	3.545	-1.415
Finance (Long)	MAPE $\downarrow$	3.758	3.531	<b>3.523</b>	4.208	<b>3.993</b>	4.045	3.789	<b>3.730</b>	<b>3.730</b>	4.307
Finance (Long)	MAE $\downarrow$	3.505	3.253	<b>3.228</b>	3.942	<b>3.594</b>	3.737	<b>3.375</b>	3.380	3.377	5.557
Weather (Short)	MSE $\downarrow$	10.673	<b>10.020</b>	10.225	10.837	10.709	<b>10.585</b>	12.213	15.192	<b>11.011</b>	6.095
Weather (Short)	MAE $\downarrow$	2.480	<b>2.389</b>	2.431	2.499	2.476	<b>2.460</b>	2.719	2.892	<b>2.469</b>	4.808
Weather (Long)	MSE $\downarrow$	13.580	13.337	<b>13.184</b>	13.577	13.424	<b>13.213</b>	16.360	<b>15.263</b>	16.434	4.101
Weather (Long)	MAE $\downarrow$	2.785	2.756	<b>2.741</b>	2.778	2.762	<b>2.754</b>	3.093	<b>2.957</b>	3.116	2.280
<b>MT-Bench: Trend Predict</b>											
Finance (Short)	3-way $\uparrow$	45.108	<b>66.849</b>	61.413	45.652	45.108	<b>59.932</b>	36.413	<b>40.217</b>	<b>40.217</b>	13.275
Finance (Short)	5-way $\uparrow$	42.935	53.261	<b>55.978</b>	40.761	<b>46.739</b>	46.233	<b>29.891</b>	17.391	17.391	2.174
Finance (Long)	3-way $\uparrow$	46.233	60.616	<b>62.671</b>	44.521	<b>58.904</b>	48.370	<b>49.658</b>	48.289	47.945	9.817
Finance (Long)	5-way $\uparrow$	40.411	<b>51.027</b>	47.945	41.438	<b>47.603</b>	45.109	41.781	<b>43.836</b>	<b>43.836</b>	6.279
Weather (Short)	Past $\uparrow$	87.363	<b>91.484</b>	89.560	82.967	83.242	<b>86.813</b>	88.189	87.088	<b>89.011</b>	2.930
Weather (Short)	Future $\uparrow$	52.198	<b>53.022</b>	<b>53.022</b>	50.275	<b>51.923</b>	49.725	<b>51.374</b>	48.626	50.824	0.640
Weather (Long)	Past $\uparrow$	87.534	<b>93.496</b>	92.141	85.637	<b>87.805</b>	82.385	<b>87.263</b>	85.637	86.992	2.620
Weather (Long)	Future $\uparrow$	49.594	<b>52.575</b>	50.136	48.781	<b>51.762</b>	49.052	<b>47.968</b>	<b>47.968</b>	47.697	1.987

Table 2. Ablation on expert modulation across backbones and tasks. Bold numbers indicate the best results within each backbone family. Avg. Imp. (%) denotes the average relative improvement of the best modulated variant over the corresponding uni-modal case (w/o EM).

additional gains in some settings, though its effects are more task- or backbone-dependent. Another notable observation is that MoME, despite employing a simple time series backbone, often outperforms MiTransformer. This suggests that, in the scenarios we study, effective cross-modal conditioning can substantially enhance predictive performance, even without highly complex time series architectures.

**Routing Pattern.** Recent studies (Chen et al., 2022; Sun et al., 2025; Guo et al., 2026) have shown that MoE models tend to route similar tokens to similar subsets of experts. We also observe that the MoME model preserves such expert specialization characteristics. As shown in Figure 3 (b), temporal tokens with similar magnitudes are often routed to similar sets of experts. However, when the RM component is activated, this specialization pattern is often interfered with. A plausible explanation is that RM reshapes the routing distribution and can substantially alter the Top-K expert set, thus weakening the effect of expert assignment. In addition to temporal magnitude, we find that the morphological shape (e.g., trends, oscillations, or abrupt changes) of temporal patterns can also play a decisive role in expert selection. A detailed discussion is included in Appendix F.

**Hyperparameters.** We conduct hyperparameter analyses on the critical design choices in our framework, including the number of activated experts  $K$ , the total number of experts  $E$ , and the number of context tokens. The results are summarized in Figure 4 (b), with additional details in Appendix D.3. The empirical results are consistent with our theoretical insights from Theorem 4.2, where a sparse activation of experts tends to result in stronger performance. In addition, we observe that a moderate number of context to-

kens achieves the best results, reflecting a trade-off between model complexity and generalization capability.

## 6. Conclusion and Future Work

We propose MoME, an MoE-based paradigm for multi-modal learning that shifts the view of cross-modal interaction from conventional token-level fusion to expert-level modulation. Across a wide range of forecasting and trend prediction tasks, MoME consistently improves over strong uni-modal and multi-modal baselines, demonstrating that expert-level modulation provides an effective mechanism for integrating auxiliary modalities.

The proposed framework suggests several promising directions for future research. While we focus on using LLM-derived textual signals to modulate time series experts, the same principle could be applied in the reverse direction. It is also possible to use temporal signals to modulate experts inside an LLM, enabling diverse tasks such as time series reasoning. In addition, MoME can naturally be generalized to more than two modalities by equipping experts with additional modulation components and jointly conditioning on multiple auxiliary signals. We believe these directions point to a broader role of expert modulation as a building block for future multi-modal learning systems.

## Impact Statement

This paper presents work whose goal is to advance the field of machine learning. There are many potential societal consequences of our work, none of which we feel must be specifically highlighted here.

## References

Akiba, T., Sano, S., Yanase, T., Ohta, T., and Koyama, M. Optuna: A next-generation hyperparameter optimization framework. In *Proceedings of the 25th ACM SIGKDD international conference on knowledge discovery & data mining*, pp. 2623–2631, 2019.

Alayrac, J.-B., Donahue, J., Luc, P., Miech, A., Barr, I., Hasson, Y., Lenc, K., Mensch, A., Millican, K., Reynolds, M., et al. Flamingo: a visual language model for few-shot learning. *Advances in neural information processing systems*, 35:23716–23736, 2022.

Alghamdi, T., Elgazzar, K., Bayoumi, M., Sharaf, T., and Shah, S. Forecasting traffic congestion using arima modeling. In *2019 15th international wireless communications & mobile computing conference (IWCMC)*, pp. 1227–1232. IEEE, 2019.

Ariyo, A. A., Adewumi, A. O., and Ayo, C. K. Stock price prediction using the arima model. In *2014 UKSim-AMSS 16th international conference on computer modelling and simulation*, pp. 106–112. IEEE, 2014.

Bao, H., Wang, W., Dong, L., Liu, Q., Mohammed, O. K., Aggarwal, K., Som, S., Piao, S., and Wei, F. Vlmo: Unified vision-language pre-training with mixture-of-modality-experts. *Advances in neural information processing systems*, 35:32897–32912, 2022.

Chang, C., Wang, W.-Y., Peng, W.-C., and Chen, T.-F. Llm4ts: Aligning pre-trained llms as data-efficient time-series forecasters. *ACM Transactions on Intelligent Systems and Technology*, 16(3):1–20, 2025.

Chen, J., Feng, A., Zhao, Z., Garza, J., Nurbek, G., Qin, C., Maatouk, A., Tassiulas, L., Gao, Y., and Ying, R. Mtbench: A multimodal time series benchmark for temporal reasoning and question answering, 2025. URL <https://arxiv.org/abs/2503.16858>.

Chen, S.-A., Li, C.-L., Arik, S. O., Yoder, N. C., and Pfister, T. TSMixer: An all-MLP architecture for time series forecasting. *Transactions on Machine Learning Research*, 2023. ISSN 2835-8856. URL <https://openreview.net/forum?id=wbpxTuXgm0>.

Chen, Z., Deng, Y., Wu, Y., Gu, Q., and Li, Y. Towards understanding the mixture-of-experts layer in deep learning. In Oh, A. H., Agarwal, A., Belgrave, D., and Cho, K. (eds.), *Advances in Neural Information Processing Systems*, 2022. URL <https://openreview.net/forum?id=MaYzugDmQV>.

DeepSeek-AI, Liu, A., Feng, B., Xue, B., et al. Deepseek-v3 technical report, 2025. URL <https://arxiv.org/abs/2412.19437>.

Fedus, W., Zoph, B., and Shazeer, N. Switch transformers: Scaling to trillion parameter models with simple and efficient sparsity. *Journal of Machine Learning Research*, 23(120):1–39, 2022.

Freeman, B. S., Taylor, G., Gharabaghi, B., and Thé, J. Forecasting air quality time series using deep learning. *Journal of the Air & Waste Management Association*, 68(8):866–886, 2018.

Guo, H., Lu, H., Nan, G., Chu, B., Zhuang, J., Yang, Y., Che, W., Cao, X., Leng, S., Cui, Q., and Jiang, X. Advancing expert specialization for better moe, 2026. URL <https://arxiv.org/abs/2505.22323>.

Ha, D., Dai, A. M., and Le, Q. V. Hypernetworks. In *International Conference on Learning Representations*, 2017. URL <https://openreview.net/forum?id=rkpACel1x>.

Han, X., Nguyen, H., Harris, C. W., Ho, N., and Saria, S. Fusemoe: Mixture-of-experts transformers for fleximodal fusion. In *The Thirty-eighth Annual Conference on Neural Information Processing Systems*, 2024. URL <https://openreview.net/forum?id=jfE7XCE89y>.

Härkönen, E., Hertzmann, A., Lehtinen, J., and Paris, S. Ganspace: Discovering interpretable gan controls. *Advances in neural information processing systems*, 33:9841–9850, 2020.

Hewamalage, H., Bergmeir, C., and Bandara, K. Recurrent neural networks for time series forecasting: Current status and future directions. *International Journal of Forecasting*, 37(1):388–427, 2021.

Hu, E. J., yelong shen, Wallis, P., Allen-Zhu, Z., Li, Y., Wang, S., Wang, L., and Chen, W. LoRA: Low-rank adaptation of large language models. In *International Conference on Learning Representations*, 2022. URL <https://openreview.net/forum?id=nZeVKeeFYf9>.

Jacobs, R. A., Jordan, M. I., Nowlan, S. J., and Hinton, G. E. Adaptive mixtures of local experts. *Neural computation*, 3(1):79–87, 1991.

Ji, J., Wang, J., Huang, C., Wu, J., Xu, B., Wu, Z., Zhang, J., and Zheng, Y. Spatio-temporal self-supervised learning for traffic flow prediction. In *Proceedings of the AAAI conference on artificial intelligence*, volume 37, pp. 4356–4364, 2023.

Jiang, A. Q., Sablayrolles, A., Roux, A., Mensch, A., Savary, B., et al. Mixtral of experts, 2024. URL <https://arxiv.org/abs/2401.04088>.

Jiang, Y., Yu, W., Lee, G., Song, D., Shin, K., Cheng, W., Liu, Y., and Chen, H. Timexl: Explainable multi-modal

time series prediction with llm-in-the-loop, 2025. URL <https://arxiv.org/abs/2503.01013>.

Jin, M., Wang, S., Ma, L., Chu, Z., Zhang, J. Y., Shi, X., Chen, P.-Y., Liang, Y., Li, Y.-F., Pan, S., and Wen, Q. Time-LLM: Time series forecasting by re-programming large language models. In *The Twelfth International Conference on Learning Representations*, 2024a. URL <https://openreview.net/forum?id=Unb5CVpta>.

Jin, M., Zhang, Y., Chen, W., Zhang, K., Liang, Y., Yang, B., Wang, J., Pan, S., and Wen, Q. Position: What can large language models tell us about time series analysis. In *Forty-first International Conference on Machine Learning*, 2024b. URL <https://openreview.net/forum?id=iroZNDxFJZ>.

Kawata, R., Matsutani, K., Kinoshita, Y., Nishikawa, N., and Suzuki, T. Mixture of experts provably detect and learn the latent cluster structure in gradient-based learning. In *Forty-second International Conference on Machine Learning*, 2025. URL <https://openreview.net/forum?id=2xmOEbpYv1>.

Koprinska, I., Wu, D., and Wang, Z. Convolutional neural networks for energy time series forecasting. In *2018 international joint conference on neural networks (IJCNN)*, pp. 1–8. IEEE, 2018.

Lai, G., Chang, W.-C., Yang, Y., and Liu, H. Modeling long-and short-term temporal patterns with deep neural networks. In *The 41st international ACM SIGIR conference on research & development in information retrieval*, pp. 95–104, 2018.

Lam, R., Sanchez-Gonzalez, A., Willson, M., Wirnsberger, P., Fortunato, M., Alet, F., Ravuri, S., Ewalds, T., Eaton-Rosen, Z., Hu, W., et al. Learning skillful medium-range global weather forecasting. *Science*, 382(6677):1416–1421, 2023.

Lei, H., Cheng, X., Qin, Q., Wang, D., Huang, H., Gu, Q., Wu, Y., and Ji, L. M3-JEPA: Multimodal alignment via multi-gate moe based on the joint-embedding predictive architecture. In *Forty-second International Conference on Machine Learning*, 2025. URL <https://openreview.net/forum?id=tYwKQMMjJA>.

Lepikhin, D., Lee, H., Xu, Y., Chen, D., Firat, O., Huang, Y., Krikun, M., Shazeer, N., and Chen, Z. {GS}hard: Scaling giant models with conditional computation and automatic sharding. In *International Conference on Learning Representations*, 2021. URL <https://openreview.net/forum?id=qrwe7XHTmYb>.

Li, J., Li, D., Savarese, S., and Hoi, S. Blip-2: Bootstrapping language-image pre-training with frozen image encoders and large language models. In *International conference on machine learning*, pp. 19730–19742. PMLR, 2023.

Lin, X. V., Shrivastava, A., Luo, L., Iyer, S., Lewis, M., Ghosh, G., Zettlemoyer, L., and Aghajanyan, A. Moma: Efficient early-fusion pre-training with mixture of modality-aware experts, 2024. URL <https://arxiv.org/abs/2407.21770>.

Liu, B., Chen, H., Sharma, A., Jiang, G., and Xiong, H. Modeling heterogeneous time series dynamics to profile big sensor data in complex physical systems. In *2013 IEEE International Conference on Big Data*, pp. 631–638. IEEE, 2013.

Liu, H., Li, C., Wu, Q., and Lee, Y. J. Visual instruction tuning. *Advances in neural information processing systems*, 36:34892–34916, 2023.

Liu, H., Xu, S., Zhao, Z., Kong, L., Prabhakar Kamarthi, H., Sasanur, A., Sharma, M., Cui, J., Wen, Q., Zhang, C., et al. Time-mmd: Multi-domain multimodal dataset for time series analysis. *Advances in Neural Information Processing Systems*, 37:77888–77933, 2024a.

Liu, H., Liu, C., and Prakash, B. A. A picture is worth a thousand numbers: Enabling llms reason about time series via visualization. In *Proceedings of the 2025 Conference of the Nations of the Americas Chapter of the Association for Computational Linguistics: Human Language Technologies (Volume 1: Long Papers)*, pp. 7486–7518, 2025a.

LIU, M., Zeng, A., Chen, M., Xu, Z., LAI, Q., Ma, L., and Xu, Q. SCINet: Time series modeling and forecasting with sample convolution and interaction. In Oh, A. H., Agarwal, A., Belgrave, D., and Cho, K. (eds.), *Advances in Neural Information Processing Systems*, 2022. URL <https://openreview.net/forum?id=AyajSjTAzmg>.

Liu, S., Yu, H., Liao, C., Li, J., Lin, W., Liu, A. X., and Dustdar, S. Pyraformer: Low-complexity pyramidal attention for long-range time series modeling and forecasting. In *International Conference on Learning Representations*, 2022. URL <https://openreview.net/forum?id=0EXmFzUn5I>.

Liu, X., Liu, J., Woo, G., Aksu, T., Liang, Y., Zimmermann, R., Liu, C., Li, J., Savarese, S., Xiong, C., and Sahoo, D. Moirai-moe: Empowering time series foundation models with sparse mixture of experts. In *Forty-second International Conference on Machine Learning*, 2025b. URL <https://openreview.net/forum?id=SrEOUSyJcR>.

Liu, Y., Hu, T., Zhang, H., Wu, H., Wang, S., Ma, L., and Long, M. itransformer: Inverted transformers are effective for time series forecasting. In *The Twelfth International Conference on Learning Representations*, 2024b. URL <https://openreview.net/forum?id=JePfAI8fah>.

Mehtab, S. and Sen, J. A time series analysis-based stock price prediction using machine learning and deep learning models. *International journal of business forecasting and marketing intelligence*, 6(4):272–335, 2020.

Neubauer, L. and Filzmoser, P. Improving forecasts for heterogeneous time series by “averaging”, with application to food demand forecasts. *International Journal of Forecasting*, 40(4):1622–1645, 2024.

Nguyen, H., Akbarian, P., Yan, F., and Ho, N. Statistical perspective of top-k sparse softmax gating mixture of experts. In *The Twelfth International Conference on Learning Representations*, 2024. URL <https://openreview.net/forum?id=jvtmdK69KQ>.

Ni, J. and Xu, Y. Forecasting the dynamic correlation of stock indices based on deep learning method. *Computational Economics*, 61(1):35–55, 2023.

Ni, R., Lin, Z., Wang, S., and Fanti, G. Mixture-of-linear-experts for long-term time series forecasting. In *International Conference on Artificial Intelligence and Statistics*, pp. 4672–4680. PMLR, 2024.

Nie, Y., Nguyen, N. H., Sinthong, P., and Kalagnanam, J. A time series is worth 64 words: Long-term forecasting with transformers. In *The Eleventh International Conference on Learning Representations*, 2023. URL <https://openreview.net/forum?id=Jbdc0vTOcol>.

Obst, D., De Vilmarest, J., and Goude, Y. Adaptive methods for short-term electricity load forecasting during covid-19 lockdown in france. *IEEE transactions on power systems*, 36(5):4754–4763, 2021.

Perez, E., Strub, F., De Vries, H., Dumoulin, V., and Courville, A. Film: Visual reasoning with a general conditioning layer. In *Proceedings of the AAAI conference on artificial intelligence*, volume 32, 2018.

Quinlan, P., Li, Q., and Zhu, X. Chat-ts: Enhancing multi-modal reasoning over time-series and natural language data, 2026. URL <https://arxiv.org/abs/2503.10883>.

Rangapuram, S. S., Seeger, M. W., Gasthaus, J., Stella, L., Wang, Y., and Januschowski, T. Deep state space models for time series forecasting. *Advances in neural information processing systems*, 31, 2018.

Shen, C., Yu, W., Zhao, Z., Song, D., Cheng, W., Chen, H., and Ni, J. Multi-modal view enhanced large vision models for long-term time series forecasting, 2025. URL <https://arxiv.org/abs/2505.24003>.

Shen, S., Yao, Z., Li, C., Darrell, T., Keutzer, K., and He, Y. Scaling vision-language models with sparse mixture of experts. In *The 2023 Conference on Empirical Methods in Natural Language Processing*, 2023. URL <https://openreview.net/forum?id=IpJ5rAFLv7>.

Shi, X., Wang, S., Nie, Y., Li, D., Ye, Z., Wen, Q., and Jin, M. Time-moe: Billion-scale time series foundation models with mixture of experts. In *The Thirteenth International Conference on Learning Representations*, 2025. URL <https://openreview.net/forum?id=elwDDFmlVu>.

Sun, C., Li, H., Li, Y., and Hong, S. TEST: Text prototype aligned embedding to activate LLM’s ability for time series. In *The Twelfth International Conference on Learning Representations*, 2024. URL <https://openreview.net/forum?id=Tuh4nZVb0g>.

Sun, Y., Xie, Z., Eldele, E., Chen, D., Hu, Q., and Wu, M. Learning pattern-specific experts for time series forecasting under patch-level distribution shift, 2025. URL <https://arxiv.org/abs/2410.09836>.

Tan, M., Merrill, M. A., Gupta, V., Althoff, T., and Hartvigsen, T. Are language models actually useful for time series forecasting? In *The Thirty-eighth Annual Conference on Neural Information Processing Systems*, 2024. URL <https://openreview.net/forum?id=DV15UbHCY1>.

Wang, W., Bao, H., Dong, L., Bjorck, J., Peng, Z., Liu, Q., Aggarwal, K., Mohammed, O. K., Singhal, S., Som, S., et al. Image as a foreign language: Beit pretraining for vision and vision-language tasks. In *Proceedings of the IEEE/CVF Conference on Computer Vision and Pattern Recognition*, pp. 19175–19186, 2023.

Wang, X., Feng, M., Qiu, J., Gu, J., and Zhao, J. From news to forecast: Integrating event analysis in LLM-based time series forecasting with reflection. In *The Thirty-eighth Annual Conference on Neural Information Processing Systems*, 2024. URL <https://openreview.net/forum?id=tj8nsfxi5r>.

wang, Y., Lei, P., Song, J., Hao, Y., Chen, T., Zhang, Y., JIA, L., Li, Y., and zhongyu wei. ITFormer: Bridging time series and natural language for multi-modal QA with large-scale multitask dataset. In *Forty-second International Conference on Machine Learning*, 2025. URL <https://openreview.net/forum?id=GByP03IitA>.

Wu, H., Xu, J., Wang, J., and Long, M. Autoformer: Decomposition transformers with auto-correlation for long-term series forecasting. In Beygelzimer, A., Dauphin, Y., Liang, P., and Vaughan, J. W. (eds.), *Advances in Neural Information Processing Systems*, 2021. URL <https://openreview.net/forum?id=J4gRj6d5Qm>.

Wu, H., Hu, T., Liu, Y., Zhou, H., Wang, J., and Long, M. Timesnet: Temporal 2d-variation modeling for general time series analysis, 2023. URL <https://arxiv.org/abs/2210.02186>.

Yang, A., Li, A., Yang, B., Zhang, B., Hui, B., et al. Qwen3 technical report, 2025. URL <https://arxiv.org/abs/2505.09388>.

Yin, X., Yan, D., Almudaifer, A., Yan, S., and Zhou, Y. Forecasting stock prices using stock correlation graph: A graph convolutional network approach. In *2021 International Joint Conference on Neural Networks (IJCNN)*, pp. 1–8. IEEE, 2021.

Zaini, N., Ean, L. W., Ahmed, A. N., and Malek, M. A. A systematic literature review of deep learning neural network for time series air quality forecasting. *Environmental Science and Pollution Research*, 29(4):4958–4990, 2022.

Zeng, A., Chen, M., Zhang, L., and Xu, Q. Are transformers effective for time series forecasting? In *Proceedings of the AAAI conference on artificial intelligence*, volume 37, pp. 11121–11128, 2023.

Zhang, G. P. Time series forecasting using a hybrid arima and neural network model. *Neurocomputing*, 50:159–175, 2003.

Zhang, J., Feng, L., Guo, X., Wu, Y., Dong, Y., and Xu, D. Timemaster: Training time-series multimodal llms to reason via reinforcement learning, 2025a. URL <https://arxiv.org/abs/2506.13705>.

Zhang, X., Han, B., Fang, H., Ansari, A. F., Zhang, S., Mad-dix, D. C., Hu, C., Wilson, A. G., Mahoney, M. W., Wang, H., Liu, Y., Rangwala, H., Karypis, G., and Wang, B. When does multimodality lead to better time series forecasting?, 2025b. URL <https://arxiv.org/abs/2506.21611>.

Zhou, H., Zhang, S., Peng, J., Zhang, S., Li, J., Xiong, H., and Zhang, W. Informer: Beyond efficient transformer for long sequence time-series forecasting. In *Proceedings of the AAAI conference on artificial intelligence*, volume 35, pp. 11106–11115, 2021.

Zhou, T., Ma, Z., Wen, Q., Wang, X., Sun, L., and Jin, R. Fedformer: Frequency enhanced decomposed transformer for long-term series forecasting. In *International conference on machine learning*, pp. 27268–27286. PMLR, 2022.

Zhou, T., Niu, P., Wang, X., Sun, L., and Jin, R. One fits all: Power general time series analysis by pretrained LM. In *Thirty-seventh Conference on Neural Information Processing Systems*, 2023. URL <https://openreview.net/forum?id=gMS6FVZvmF>.

## A. Detailed Theoretical Analysis

### A.1. Proof of Lemma 4.1

Consider an MLP layer of the following form

$$f(\mathbf{x}) = \mathbf{W}^{(d)} (\sigma(\mathbf{W}^{(u)} \mathbf{x}) \odot (\mathbf{W}^{(g)} \mathbf{x})),$$

where  $\mathbf{W}^{(u)}, \mathbf{W}^{(g)} \in \mathbb{R}^{m \times d}$  and  $\mathbf{W}^{(d)} \in \mathbb{R}^{r \times m}$  are weight matrices,  $\mathbf{x} \in \mathbb{R}^d$  is the hidden state,  $\sigma(\cdot)$  is a nonlinear activation, and  $\odot$  denotes element-wise multiplication.

Let the hidden dimension  $m$  be partitioned into  $n$  groups of size  $c$  (so that  $m = n \times c$ ).

For each group  $i = 1, \dots, n$ , denote the corresponding submatrices  $\mathbf{W}_i^{(u)}, \mathbf{W}_i^{(g)} \in \mathbb{R}^{c \times d}$  and  $\mathbf{W}_i^{(d)} \in \mathbb{R}^{r \times c}$ . Then we need to prove that the layer output can be expressed as a sum of  $n$  sub-modules:

$$f(\mathbf{x}) = \sum_{i=1}^n f_i(\mathbf{x}) = \sum_{i=1}^n \mathbf{W}_i^{(d)} (\sigma(\mathbf{W}_i^{(u)} \mathbf{x}) \odot (\mathbf{W}_i^{(g)} \mathbf{x})).$$

First, we denote

$$z(\mathbf{x}) := \sigma(\mathbf{W}^{(u)} \mathbf{x}) \odot (\mathbf{W}^{(g)} \mathbf{x}).$$

Since  $\sigma(\cdot)$  is an element-wise nonlinear activation function, and  $\odot$  is an element-wise product, above equation can be partitioned into block-wise calculation as:

$$\begin{aligned} z(\mathbf{x}) &= \begin{bmatrix} \sigma(\mathbf{W}_1^{(u)}(\mathbf{x})) \\ \vdots \\ \sigma(\mathbf{W}_n^{(u)}(\mathbf{x})) \end{bmatrix} \odot \begin{bmatrix} \mathbf{W}_1^{(g)}(\mathbf{x}) \\ \vdots \\ \mathbf{W}_n^{(g)}(\mathbf{x}) \end{bmatrix} \\ &= \begin{bmatrix} [\sigma(\mathbf{W}_1^{(u)}(\mathbf{x})) \odot \mathbf{W}_1^{(g)}(\mathbf{x})] \\ \vdots \\ [\sigma(\mathbf{W}_n^{(u)}(\mathbf{x})) \odot \mathbf{W}_n^{(g)}(\mathbf{x})] \end{bmatrix}. \end{aligned}$$

Therefore,  $z(\mathbf{x}) \in \mathbb{R}^n$  can be partitioned into  $n$  contiguous blocks of length  $c$ :

$$z(\mathbf{x}) = \begin{bmatrix} z_1(\mathbf{x}) \\ \vdots \\ z_n(\mathbf{x}) \end{bmatrix}, \quad z_i(\mathbf{x}) \in \mathbb{R}^c, \quad i = 1, \dots, n.$$

Specifically,

$$z_i(\mathbf{x}) = \sigma(\mathbf{W}_i^{(u)} \mathbf{x}) \odot (\mathbf{W}_i^{(g)} \mathbf{x}), \quad i = 1, \dots, n.$$

Similarly, we partition  $\mathbf{W}^{(d)}$  column-wise into matching blocks

$$\mathbf{W}^{(d)} = \begin{bmatrix} \mathbf{W}_1^{(d)} & \dots & \mathbf{W}_n^{(d)} \end{bmatrix}, \quad \mathbf{W}_i^{(d)} \in \mathbb{R}^{r \times c}.$$

Then matrix multiplication can be written as the following blockwise expansion:

$$f(\mathbf{x}) = \mathbf{W}^{(d)} z(\mathbf{x}) = \sum_{i=1}^n \mathbf{W}_i^{(d)} z_i(\mathbf{x}).$$

Altogether, we have:

$$f(\mathbf{x}) = \sum_{i=1}^n \mathbf{W}_i^{(d)} (\sigma(\mathbf{W}_i^{(u)} \mathbf{x}) \odot (\mathbf{W}_i^{(g)} \mathbf{x})) = \sum_{i=1}^n f_i(\mathbf{x}),$$

which is the desired decomposition.

## A.2. Proof of Theorem 4.2

A fully-activated MoE with  $E$  experts can be expressed as

$$\text{MoE}_D(\mathbf{x}) = \sum_{i=1}^E g_i(\mathbf{x}) f_i(\mathbf{x}).$$

A sparse MoE under Top-K activation can be denoted as

$$\text{MoE}_S(\mathbf{x}) = \sum_{i \in \mathcal{A}} g_i(\mathbf{x}) f_i(\mathbf{x}) = \sum_{i=1}^E \lambda_i g_i(\mathbf{x}) f_i(\mathbf{x}),$$

where  $\sum_i \lambda_i = K$ ,  $\lambda_i = \{0, 1\}$  denotes the binary mask for expert selection and  $\mathcal{A}$  denotes the set of activated experts ( $|\mathcal{A}| = K$ ), then the amount of truncated information is

$$\begin{aligned} \mathcal{L}(\mathbf{x}) &= \|\text{MoE}_D(\mathbf{x}) - \text{MoE}_S(\mathbf{x})\|^2 \\ &= \left\| \sum_{i=1}^E g_i(\mathbf{x}) f_i(\mathbf{x}) - \sum_{i \in \mathcal{A}} g_i(\mathbf{x}) f_i(\mathbf{x}) \right\|^2 \\ &= \left\| \sum_{i \notin \mathcal{A}} g_i(\mathbf{x}) f_i(\mathbf{x}) \right\|^2 \end{aligned}$$

The above equation can be reorganized into vector notations. Let  $\mathcal{I} := \{1, \dots, E\} \setminus \mathcal{A}$  be the index set of pruned experts, so that  $|\mathcal{I}| = E - K$ . Then, we define

$$\begin{aligned} \mathbf{g}(\mathbf{x}) &:= (g_i(\mathbf{x}))_{i \in \mathcal{I}} \in \mathbb{R}^{E-K} \\ \mathbf{f}(\mathbf{x}) &:= [f_i(\mathbf{x})]_{i \in \mathcal{I}} \in \mathbb{R}^{d \times (E-K)}, \end{aligned}$$

where  $d$  is the dimension of the latent space. Let us denote

$$\mathbf{F}(\mathbf{x}) = \mathbf{f}^\top(\mathbf{x}) \mathbf{f}(\mathbf{x}) \in \mathbb{R}^{(E-K) \times (E-K)},$$

where  $\mathbf{F}_{ij}(\mathbf{x}) = \langle f_i(\mathbf{x}), f_j(\mathbf{x}) \rangle$ , be the corresponding gram matrix. Then, we have

$$\begin{aligned} \mathcal{L}(\mathbf{x}) &= \|\mathbf{f}(\mathbf{x}) \mathbf{g}(\mathbf{x})\|^2 \\ &= \langle \mathbf{f}(\mathbf{x}) \mathbf{g}(\mathbf{x}), \mathbf{f}(\mathbf{x}) \mathbf{g}(\mathbf{x}) \rangle \\ &= \mathbf{g}^\top(\mathbf{x}) \mathbf{f}^\top(\mathbf{x}) \mathbf{f}(\mathbf{x}) \mathbf{g}(\mathbf{x}) \\ &= \mathbf{g}^\top(\mathbf{x}) \mathbf{F}(\mathbf{x}) \mathbf{g}(\mathbf{x}). \end{aligned}$$

Recall that a Rayleigh quotient is defined as

$$R(\mathbf{F}, \mathbf{g}) = \frac{\mathbf{g}^\top \mathbf{F} \mathbf{g}}{\mathbf{g}^\top \mathbf{g}}.$$

Since  $\mathbf{F}(\mathbf{x})$  is symmetric positive semi-definite, the Rayleigh quotient implies that

$$\mathbf{g}^\top(\mathbf{x}) \mathbf{F}(\mathbf{x}) \mathbf{g}(\mathbf{x}) \leq \gamma_{\max}(\mathbf{F}) \|\mathbf{g}(\mathbf{x})\|^2, \quad (6)$$

where  $\gamma_{\max}$  stands for the largest eigenvalue of the matrix  $\mathbf{F}(\mathbf{x})$ . By the Gershgorin circle theorem, for every eigenvalue  $\gamma$  of  $\mathbf{F}(\mathbf{x})$ , we have the inequality:

$$|\gamma - \mathbf{F}_{ii}| \leq \sum_{j \neq i} |\mathbf{F}_{ij}| \leq (E - K - 1)\mu$$

The maximum eigenvalue also suffices for the inequality.

$$\Rightarrow |\gamma_{\max} - \mathbf{F}_{ii}| \leq (E - K - 1)\mu.$$

Using this bounding and the initial assumption ( $\|f_i(\mathbf{x})\| \leq B$ , for  $\forall i$ ), we have

$$\begin{aligned} |\gamma_{\max}| &\leq |\mathbf{F}_{ii}| + (E - K - 1)\mu \\ |\gamma_{\max}| &\leq B^2 + (E - K - 1)\mu. \end{aligned}$$

Substituting this inequality into Equation (6), we obtain

$$\mathcal{L}(\mathbf{x}) \leq [B^2 + (E - K - 1)\mu] \sum_{i \notin \mathcal{A}} g_i(\mathbf{x})^2,$$

which completes the proof.

## B. MoE for Pure Time Series Models

In this section, MoE modules are integrated into several representative uni-modal time series backbones for multiple purposes. First, they demonstrate the flexibility of MoE, which can be seamlessly integrated into diverse architectures, yielding consistent performance improvements. Second, they complement the theoretical insights of Theorem 4.2 by experimentally showing that a sparse activation of experts is more likely to achieve the best performance. Third, they allow us to investigate the dynamic of token routing behavior (presented in Appendix F). Finally, these implementations provide a foundation for future research, where the proposed expert modulation can be extended to a broader range of backbone architectures.

### B.1. MoE for Time Series Model

Most existing MoE-based time series models simply replace the MLP layers within a Transformer backbone with MoE blocks (Liu et al., 2025b; Shi et al., 2025). However, we highlight a more general principle: **any token-wise function can be expressed in an MoE form**.

Time series backbone models typically include some form of token-wise mapping during the forward pass:

$$f(\mathbf{x}) : \mathbb{R}^d \rightarrow \mathbb{R}^d, \quad f(\mathbf{x}) : \mathbb{R}^L \rightarrow \mathbb{R}^{L'},$$

where  $d, L, L'$  denotes the hidden dimension and the length of temporal windows, respectively. The mapping  $f(\cdot)$  can be MLP blocks, linear projectors, or feed-forward components within the attention layers.

Nevertheless, to construct the MoE variants, we can simply replace  $h(\cdot)$  with its MoE counterpart:

$$\text{MoE}(\mathbf{x}) = \sum_{i=1}^E \lambda_i(\mathbf{x}) g_i(\mathbf{x}) f_i(\mathbf{x}),$$

where  $g_i(\mathbf{x})$  denotes the gating score,  $\lambda_i(\mathbf{x}) \in \{0, 1\}$  is the Top-K binary selection mask, and  $E_i$  is the  $i$ -th expert function. This viewpoint implies that MoE is not limited to substituting MLPs; rather, it provides a general framework for decomposing any token-wise transformation into a set of specialized expert functions.

### B.2. Backbone-Specific Implementations

Following the general construction principle described above, we instantiate MoE modules within several representative time series backbones spanning different architectural families: (1) linear models (DLinear (Zeng et al., 2023)), (2) MLP-based models (TSMixer (Chen et al., 2023)), and (3) transformer-based models (iTransformer (Liu et al., 2024b)). Specifically, in DLinear, we replace the per-channel linear mappings in both the seasonal and trend components with Linear-Experts MoE modules (Algorithm 1). In TSMixer, the time-mixing MLP is replaced by MLP-Experts MoE modules, while the channel-mixing block is unchanged (Algorithm 2). In iTransformer, the feed-forward layers in the inverted transformer architecture are similarly replaced by MLP-Experts MoE modules (Algorithm 3). These instantiations showcase that MoE can be flexibly integrated into diverse backbones, and also allow us to examine how MoE interacts with different computational structures.

### B.3. Results

We evaluate the proposed MoE variants across six widely used time series forecasting benchmarks, with the full results reported in Table 3. Across all settings, MoE tends to improve performance over the corresponding backbone

### Algorithm 1 DLinear-MoE

**Input:** History window  $X \in \mathbb{R}^{L \times C}$ ; horizon  $H$ ; MA kernel  $k$ ; total number of experts  $M$ ; activated experts  $K$ .  
**Output:** Forecast  $\hat{Y} \in \mathbb{R}^{H \times C}$ .

#### Seasonal-Trend decomposition (per channel)

$T \leftarrow$  Moving Average $_k(X)$

$S \leftarrow X - T$

#### Per-channel linear projections (map $L \rightarrow H$ )

**if**  $use\_moe$  **then**

$$\begin{aligned} g_i^S &\leftarrow \text{Gate}_S(S^\top) \in \mathbb{R}^{C \times M} \\ \lambda_i^S &\leftarrow \text{TopK-Mask}(g_i^S, K) \\ // \quad \lambda_{i,m}^S &\in \{0, 1\} \text{ and } \sum_{m=1}^M \lambda_{i,m}^S = K \\ \tilde{Y}_S &\leftarrow \sum_{m=1}^M \lambda_{i,m}^S \cdot g_{i,m}^S \cdot \text{Linear}_{S,m}(S^\top) \\ g_i^T &\leftarrow \text{Gate}_T(T^\top) \in \mathbb{R}^{C \times M} \\ \lambda_i^T &\leftarrow \text{TopK-Mask}(g_i^T, K) \\ // \quad \lambda_{i,m}^T &\in \{0, 1\} \text{ and } \sum_{m=1}^M \lambda_{i,m}^T = K \\ \tilde{Y}_T &\leftarrow \sum_{m=1}^M \lambda_{i,m}^T \cdot g_{i,m}^T \cdot \text{Linear}_{T,m}(T^\top) \end{aligned}$$

**else**

$$\begin{aligned} \tilde{Y}_S &\leftarrow \text{Linear}_S(S^\top) \in \mathbb{R}^{C \times H} \\ \tilde{Y}_T &\leftarrow \text{Linear}_T(T^\top) \in \mathbb{R}^{C \times H} \end{aligned}$$

**Combination**  $\hat{Y} \leftarrow (\tilde{Y}_S + \tilde{Y}_T)^\top \in \mathbb{R}^{H \times C}$

models, despite substantial differences in model capacity and architectural design. This suggests that MoE acts as a backbone-agnostic enhancement rather than an architecture-specific modification. Notably, linear models such as DLinear often exhibit the largest relative gains in certain settings, indicating that expert-based decomposition might be more beneficial for lightweight time series backbone models. We also conduct zero-shot forecasting experiments on the ETT benchmarks, and the complete results are summarized in Table 4. MoE continues to provide consistent performance improvements, demonstrating its generalization capability.

Beyond performance gains, we analyze the role of sparsity in MoE routing. Figure 5 (a) shows that fully activated MoE variants do not outperform sparse Top-K routing, as evaluated on the Electricity and Traffic datasets using TSMixer-MoE and iTransformer-MoE. This observation supports our theoretical insights in Theorem 4.2, where sparsity might improve performance by suppressing noisy signals.

### B.4. Hyperparameter Searching

For the experiments on uni-modal time series MoE models, **Optuna** (Akiba et al., 2019), a widely-used framework for efficient hyperparameter search, is first used to automatically tune hyperparameters for the baselines. Then, under the same hyperparameter setting, the MoE function is activated to test the performance for the MoE model variants. The

Dataset	h	TSMixer				DLinear				iTransformer				Avg Imp (%)	
		Original		+ MoE		Original		+ MoE		Original		+ MoE			
		MSE	MAE												
ETTm1	96	0.294	0.345	<b>0.288</b>	<b>0.343</b>	<b>0.286</b>	<b>0.335</b>	0.304	0.348	0.320	0.368	<b>0.318</b>	<b>0.364</b>	-0.95	
	192	<b>0.327</b>	<b>0.359</b>	0.331	0.369	<b>0.327</b>	<b>0.359</b>	0.334	0.367	0.361	0.391	<b>0.357</b>	<b>0.389</b>	-1.12	
	336	<b>0.374</b>	0.394	<b>0.374</b>	0.398	<b>0.367</b>	<b>0.381</b>	<b>0.367</b>	<b>0.381</b>	<b>0.393</b>	<b>0.411</b>	0.396	<b>0.411</b>	-0.29	
	720	<b>0.429</b>	<b>0.424</b>	<b>0.429</b>	0.429	<b>0.428</b>	<b>0.417</b>	0.439	0.434	0.448	0.439	<b>0.442</b>	<b>0.438</b>	-1.04	
ETTm2	96	<b>0.168</b>	<b>0.255</b>	0.170	<b>0.255</b>	0.179	0.274	<b>0.177</b>	<b>0.265</b>	0.181	0.273	<b>0.180</b>	<b>0.272</b>	0.67	
	192	0.234	0.300	<b>0.228</b>	<b>0.296</b>	<b>0.241</b>	0.317	<b>0.241</b>	<b>0.313</b>	0.249	0.317	<b>0.247</b>	<b>0.314</b>	1.15	
	336	<b>0.278</b>	<b>0.332</b>	0.280	<b>0.332</b>	0.399	0.417	<b>0.297</b>	<b>0.349</b>	0.299	0.347	<b>0.294</b>	<b>0.344</b>	7.28	
	720	<b>0.398</b>	0.406	<b>0.398</b>	<b>0.404</b>	0.738	0.562	<b>0.430</b>	<b>0.438</b>	0.376	0.397	<b>0.369</b>	<b>0.392</b>	12.24	
ETTh1	96	0.392	0.411	<b>0.383</b>	<b>0.407</b>	0.379	0.399	<b>0.375</b>	<b>0.396</b>	0.402	0.418	<b>0.393</b>	<b>0.414</b>	1.38	
	192	0.419	0.430	<b>0.415</b>	<b>0.427</b>	0.422	0.429	<b>0.411</b>	<b>0.421</b>	0.441	0.442	<b>0.434</b>	<b>0.441</b>	1.32	
	336	0.442	<b>0.441</b>	<b>0.438</b>	0.444	0.451	<b>0.448</b>	<b>0.446</b>	<b>0.448</b>	0.453	0.454	<b>0.443</b>	<b>0.448</b>	0.81	
	720	0.508	0.496	<b>0.487</b>	<b>0.488</b>	0.490	0.489	<b>0.485</b>	0.499	0.472	0.484	<b>0.468</b>	<b>0.479</b>	1.11	
ETTh2	96	<b>0.313</b>	0.366	<b>0.313</b>	<b>0.364</b>	0.370	0.393	0.302	<b>0.360</b>	0.319	0.372	<b>0.310</b>	<b>0.367</b>	5.25	
	192	0.360	0.395	<b>0.358</b>	<b>0.394</b>	0.495	0.466	<b>0.391</b>	<b>0.417</b>	0.375	0.413	<b>0.374</b>	<b>0.411</b>	5.51	
	336	0.390	0.417	<b>0.376</b>	<b>0.412</b>	0.595	0.524	<b>0.410</b>	<b>0.436</b>	<b>0.398</b>	<b>0.428</b>	<b>0.398</b>	<b>0.428</b>	8.78	
	720	<b>0.414</b>	<b>0.437</b>	0.417	0.438	0.888	0.656	<b>0.833</b>	<b>0.649</b>	0.426	0.452	<b>0.421</b>	<b>0.448</b>	1.39	
EXR	96	0.099	0.228	<b>0.095</b>	<b>0.222</b>	0.089	0.218	<b>0.081</b>	<b>0.205</b>	0.110	0.240	<b>0.106</b>	<b>0.237</b>	4.42	
	192	<b>0.196</b>	<b>0.320</b>	<b>0.196</b>	0.321	<b>0.172</b>	0.313	<b>0.172</b>	<b>0.309</b>	0.236	0.354	<b>0.227</b>	<b>0.348</b>	1.08	
	336	0.369	0.446	<b>0.352</b>	0.439	0.334	0.444	<b>0.332</b>	<b>0.434</b>	0.405	0.477	<b>0.401</b>	<b>0.471</b>	1.88	
	720	0.965	0.740	<b>0.881</b>	<b>0.716</b>	0.879	0.728	<b>0.767</b>	<b>0.659</b>	0.849	0.698	<b>0.802</b>	<b>0.673</b>	7.21	
ECL	96	0.139	0.238	<b>0.138</b>	<b>0.235</b>	0.136	<b>0.233</b>	<b>0.135</b>	<b>0.233</b>	0.164	0.271	<b>0.160</b>	<b>0.264</b>	1.29	
	192	0.161	<b>0.257</b>	<b>0.159</b>	<b>0.257</b>	<b>0.151</b>	0.248	<b>0.151</b>	<b>0.246</b>	0.185	0.289	<b>0.179</b>	<b>0.281</b>	1.34	
	336	0.171	0.271	<b>0.167</b>	<b>0.267</b>	<b>0.166</b>	0.265	0.168	<b>0.265</b>	0.201	0.304	<b>0.194</b>	<b>0.294</b>	1.56	
	720	0.200	0.294	<b>0.192</b>	<b>0.287</b>	<b>0.203</b>	0.300	<b>0.203</b>	<b>0.298</b>	0.239	0.333	<b>0.228</b>	<b>0.321</b>	2.54	
TRF	96	0.386	0.273	<b>0.378</b>	<b>0.273</b>	0.427	0.302	<b>0.401</b>	<b>0.278</b>	0.374	0.276	<b>0.371</b>	<b>0.271</b>	3.73	
	192	0.414	0.289	<b>0.399</b>	<b>0.276</b>	0.441	0.308	<b>0.422</b>	<b>0.286</b>	0.400	0.285	<b>0.379</b>	<b>0.283</b>	3.50	
	336	0.431	0.302	<b>0.410</b>	<b>0.283</b>	0.455	0.317	<b>0.439</b>	<b>0.294</b>	0.415	0.294	<b>0.406</b>	<b>0.287</b>	4.41	
	720	0.463	0.328	<b>0.450</b>	<b>0.312</b>	0.487	0.335	<b>0.465</b>	<b>0.313</b>	0.452	0.321	<b>0.448</b>	<b>0.311</b>	3.80	

Overall Avg Imp (%): 2.83

Table 3. Performance comparison of MoE integration across different models and datasets.

Dataset	h	TSMixer		TSMixer (MoE)		DLinear		DLinear (MoE)		iTransformer		iTransformer (MoE)		Imp (%)	
		MSE	MAE	MSE	MAE	MSE	MAE	MSE	MAE	MSE	MAE	MSE	MAE		
ETTh1 → ETTh2	96	0.304	0.358	<b>0.302</b>	<b>0.357</b>	0.310	0.371	<b>0.292</b>	<b>0.355</b>	0.288	0.353	<b>0.284</b>	<b>0.351</b>	2.617	1.720
	336	0.382	0.418	<b>0.380</b>	<b>0.414</b>	0.443	0.471	<b>0.432</b>	<b>0.450</b>	0.394	0.419	<b>0.375</b>	<b>0.409</b>	2.610	2.600
ETTh2 → ETTh1	96	0.519	0.483	<b>0.513</b>	<b>0.483</b>	0.459	0.450	<b>0.424</b>	0.430	<b>0.617</b>	0.542	0.619	<b>0.541</b>	2.819	1.543
	336	0.761	0.605	<b>0.639</b>	<b>0.552</b>	0.503	0.488	<b>0.460</b>	<b>0.460</b>	0.832	0.647	<b>0.787</b>	<b>0.628</b>	9.996	5.812
ETTh2 → ETTm1	96	0.724	<b>0.656</b>	<b>0.719</b>	0.661	0.737	0.657	<b>0.715</b>	<b>0.647</b>	1.017	0.772	<b>0.991</b>	<b>0.762</b>	2.077	0.685
	336	1.037	0.777	<b>1.019</b>	<b>0.771</b>	1.174	0.817	<b>0.925</b>	<b>0.741</b>	1.310	0.854	<b>1.275</b>	<b>0.843</b>	8.539	3.788
ETTh1 → ETTm2	96	0.889	0.672	<b>0.872</b>	<b>0.667</b>	0.990	0.703	<b>0.928</b>	<b>0.685</b>	1.022	0.717	<b>1.015</b>	<b>0.716</b>	2.954	1.148
	336	1.338	0.841	<b>1.306</b>	<b>0.834</b>	1.563	0.907	<b>1.538</b>	<b>0.901</b>	1.371	0.855	<b>1.363</b>	<b>0.851</b>	1.525	0.653
ETTm1 → ETTm2	96	0.192	0.275	<b>0.182</b>	<b>0.164</b>	0.186	0.278	<b>0.183</b>	<b>0.275</b>	0.209	0.285	<b>0.203</b>	<b>0.282</b>	3.230	14.166
	336	0.299	0.341	<b>0.293</b>	<b>0.339</b>	<b>0.307</b>	<b>0.371</b>	0.316	0.376	0.329	0.358	<b>0.325</b>	<b>0.357</b>	0.097	-0.161
ETTm2 → ETTm1	96	0.530	0.464	<b>0.487</b>	<b>0.448</b>	0.384	0.400	<b>0.373</b>	<b>0.390</b>	<b>0.521</b>	<b>0.474</b>	<b>0.521</b>	<b>0.474</b>	3.659	1.982
	336	0.951	0.642	<b>0.618</b>	<b>0.523</b>	0.445	0.442	<b>0.445</b>	<b>0.439</b>	<b>0.600</b>	<b>0.520</b>	0.605	0.525	11.394	6.084
Avg Imp.														4.293	3.335

Table 4. Zero-shot performance on ETT datasets. The best results between Original and the MoE variant for each model are in bold.

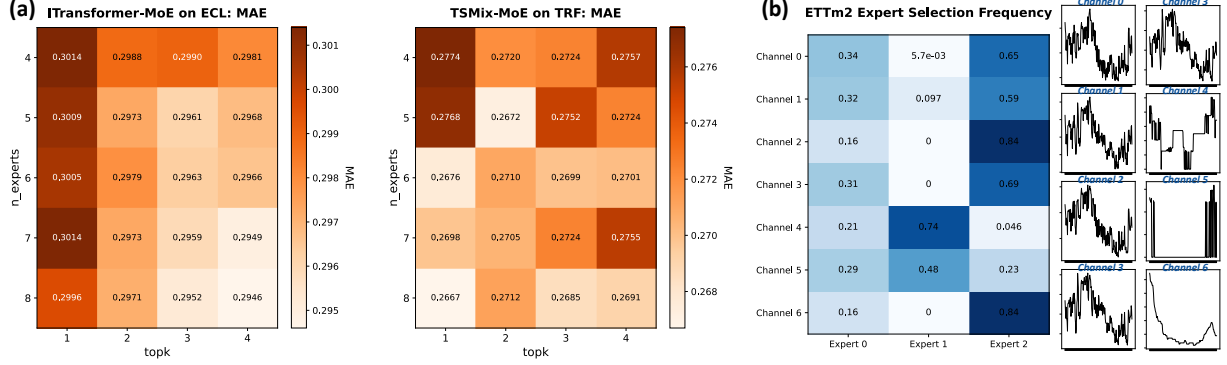


Figure 5. (a): empirical results that show sparse expert activation yields better performance than dense activation; (b): expert selection behavior for MoE-based model on ETTm2 datasets, where a channel is considered as a token.

### Algorithm 2 TSMixer-MoE

**Input:** History window  $X \in \mathbb{R}^{L \times C}$ ; horizon  $H$ ; layers  $N$ ; total number of experts  $M$ ; activated experts  $K$ .

**Output:** Forecast  $\hat{Y} \in \mathbb{R}^{H \times C}$ .

```

 $Z_0 \leftarrow X$ 
for  $i = 1$  to  $N$  do
    // Time-Mixing
    if use_moe then
         $\tilde{Z} \leftarrow \text{LN}(Z_{i-1})^\top \in \mathbb{R}^{C \times L}$ 
         $g_i \leftarrow \text{Gate}_{\text{time}}(\tilde{Z}) \in \mathbb{R}^{C \times M}$ 
         $\lambda_i \leftarrow \text{TopK-Mask}(g_i, K)$ 
        //  $\lambda_{i,m} \in \{0, 1\}$  and  $\sum_{m=1}^M \lambda_{i,m} = K$ 
         $U \leftarrow \left( \sum_{m=1}^M \lambda_{i,m} \cdot g_{i,m} \cdot \text{MLP}_{\text{time},m}(\tilde{Z}) \right)^\top$ 
    else
         $U \leftarrow \text{MLP}_{\text{time}}(\text{LN}(Z_{i-1})^\top)^\top$ 
     $Z_i \leftarrow Z_{i-1} + U$ 
    // Channel-Mixing
     $V \leftarrow \text{MLP}_{\text{channel}}(\text{LN}(Z_i))$ 
     $Z_i \leftarrow Z_i + V$ 
Projection  $\hat{Y} \leftarrow \text{Head}(Z_N^\top)^\top \in \mathbb{R}^{H \times C}$ 

```

### Algorithm 3 iTransformer-MoE

**Input:** History window  $X \in \mathbb{R}^{L \times C}$  (length  $L$ , channels  $C$ ); forecast horizon  $H$ ; hidden dimension  $d$ ; layer  $N$ ; total number of experts  $M$ ; activated experts  $K$ .

**Output:** Forecast  $\hat{Y} \in \mathbb{R}^{H \times C}$ .

#### Invert Tokens (time $\leftrightarrow$ variables)

```

 $\tilde{X} \leftarrow \text{Transpose}(X) \in \mathbb{R}^{C \times L}$ 
 $\tilde{Z}_0 \leftarrow \text{Linear}(\tilde{X}) + \text{PosEnc}(1:C)$ 

```

**Inverted-Encoder (operate on channels)** **for**  $i = 1$  **to**  $N$  **do**

```

 $\tilde{Z}_i \leftarrow \text{MSA}(\tilde{Z}_{i-1})$ 
if use_moe then
     $g_i \leftarrow \text{Gate}(\tilde{Z}_i) \in \mathbb{R}^{C \times M}$ 
     $\lambda_i \leftarrow \text{TopK-Mask}(g_i, K)$ 
    //  $\lambda_{i,m} \in \{0, 1\}$  and  $\sum_{m=1}^M \lambda_{i,m} = K$ 
     $H_i \leftarrow \sum_{m=1}^M \lambda_{i,m} \cdot g_{i,m} \cdot \text{Expert}_m(\tilde{Z}_i)$ 
else
     $H_i \leftarrow \text{FFN}(\tilde{Z}_i)$ 
 $\tilde{Z}_i \leftarrow \tilde{Z}_i + H_i$ 

```

**Projection**  $\hat{Y} \leftarrow \text{Head}(\tilde{Z}_N) \in \mathbb{R}^{C \times H}$

following hyperparameters are optimized:

`learning_rate`  $\sim \mathcal{U}(1e-5, 5e-3)$ ,

`dropout`  $\sim \mathcal{U}(0.0, 0.6)$ ,

`d_model`  $\in \{16, 32, 64, 128\}$ ,

`n_heads`  $\in \{2, 4, 8\}$ ,

`n_layers`  $\in [2, 6]$ ,

`patch_len`  $\in \{8, 16, 32\}$ ,

`stride`  $\in \{4, 8, 16\}$ .

The search direction is set to minimize the MSE on the validation set, and `MedianPruner` is utilized for early stopping. A total of 30 trials are run per experiment. In addition, random seeds are also fixed for consistent behavior.

## C. Datasets Preparation

### C.1. MT-Bench

MT-Bench datasets provide paired time series and text of news reports. A detailed summary of all subsets is provided in Table 5. We provide a detailed discussion for each of

Domain	Target	Dimension	Frequency	Number of Samples	Window per Sample
MT-Weather (Short)	Temperature	1	1-hour	1820	7 Days → 1 Day
MT-Weather (Long)	Temperature	1	1-hour	1841	14 Days → 3 Days
MT-Finance (Short)	Stock Price	1	5-min	916	7 Days → 1 Day
MT-Finance (Long)	Stock Price	1	1-hour	1458	30 Days → 7 Days

Table 5. Overview of numerical data in MT-Bench.

Domain	Target	Dimension	Frequency	Number of Timestamps	Window per Sample
Environment	Air Quality	4	Daily	11102	7 Days → 1 Day
Energy	Gasoline Prices	9	Weekly	1479	14 Days → 3 Days
Health (US)	Influenza Patients Proportion	11	Weekly	1389	14 Days → 3 Days
Health (AFR)	Influenza Patients Proportion	11	Weekly	1389	14 Days → 3 Days
Social Good	Unemployment Rate	1	Monthly	900	14 Days → 3 Days

Table 6. Overview of numerical data in Time-MMD for selected domains: Climate, Energy, Health (US/AFR), and Social Good.

Dataset	Target	Dimension	Number of Timestamps	Frequency
ETTh1 / ETTh2	Oil Temperature	7	17,420	1 hour
ETTm1 / ETTm2	Oil Temperature	7	69,680	15 min
Electricity	Electricity Consumption	321	26,304	1 hour
Traffic	Road Occupancy Rate	862	17,544	1 hour

Table 7. Classical uni-modal time series forecasting datasets.

3-way Label	5-way Label	Financial Price	Weather Temperature	
Negative	Bearish Warning	< -4% -4% ~ -2%	Past: < -0.25	Future: < -1.5
Neutral	Neutral	-2% ~ 2%	Past: -0.25 ~ 0.25	Future: -1.5 ~ 1.5
Positive	Growth-Oriented Bullish	2% ~ 4% > 4%	Past: > 0.25	Future: > 1.5

Table 8. Trend label binning for MT-Finance and MT-Weather data.

them in the following sections.

**MT-Finance.** The MT-Finance dataset is constructed from single-channel stock price time series, where each sample consists of a historical observation window paired with a future prediction target, which can be either an overall price trend or a precise price series forecasting. Detailed information on trend labels is provided in Table 8. We evaluated two prediction settings that differ in temporal resolution and prediction horizon.

In the short-term prediction, the model receives 7 days of 5-minutes-sampled stock prices and predicts either the next-day closing price or the short-term price trend. This setting primarily captures local fluctuations and intraday volatility. In the long-term setting, the model observes 30 days of hourly-sampled stock prices and predicts the price for the next 7 days. Although this task spans a longer temporal range, the lower sampling frequency results in fewer observed timestamps than in the short-term setting. Therefore, this setting emphasizes modeling slow-evolving market trends rather than abrupt changes.

Each time series is paired with a news context that describes recent market events. However, textual information might sometimes be inconsistent with the actual future market movement. In mimicking the real-world scenario, we deliberately incorporated inconsistent textual pairs in both training and test sets. Specifically, we control the ratio of consistent vs. inconsistent news at approximately 80% : 20%. After pre-processing, the short-term dataset contains 916 samples and the long-term one contains 1,458 samples.

**MT-Weather.** The MT-Weather dataset contains a single-channel time series of the daily mean temperature recorded at multiple geographic locations. Each location is treated as an independent series. Similarly to MT-Finance, we constructed two prediction settings that differ in temporal resolutions and prediction horizon.

In the short-term setting, the model will observe 7 days of hourly-sampled temperature values and predict the temperature of the next day. This setting reflects short-range weather variability, which is primarily driven by local meteorological conditions. The short-term dataset contains 1,820 samples after filtering. In the long-term setting, the model will observe 14 days of hourly-sampled temperature data and predict the average temperature for the next 3 days (or overall trend of the next 3 days). The long-term dataset contains a total of 1,841 samples.

**Trend Label Assignment.** To analyze directional movement in time series, we convert each continuous forecasting sample into a discrete trend label for trend prediction.

For finance time series, the percentage price change over

the prediction window is measured

$$\Delta_{\text{finance}} = \frac{y_{\text{end}} - y_{\text{start}}}{y_{\text{start}}}.$$

This value reflects whether the stock price increased, decreased, or remained stable in the future.

For weather time series, trend definition differs between past and future prediction tasks. For past trend analysis, we downsample the input sequence (e.g., 7 days) into daily means and compute a linear slope

$$\Delta_{\text{past}} = \text{slope}(\{\bar{x}_i\}_{i=1}^L).$$

This reflects the general direction of recent temperature movement. For future trend prediction, the future horizon is too short to reliably estimate a slope. So, we instead define the trend as the mean temperature difference between the last input day and the future window

$$\Delta_{\text{future}} = \text{Mean}(\{\bar{x}_i\}_{i=1}^T) - \text{Mean}(\{\bar{x}_j\}_{j=1}^L).$$

After computing the continuous trend values above, we discretize them into categorical labels. For MT-Finance, we support both 3-way and 5-way classification, while we use only 3-way classification for MT-Weather. All threshold values used for binning are summarized in Table 8.

## C.2. TimeMMD

**Short-Term Prediction.** We adopt the time series data from (Liu et al., 2024a) but redefine the task as short-term forecasting. We reckon such a setting to be more reasonable and appropriate given the non-stationary nature of the underlying data (see Table 6 for dataset details). For example, Environment data consists of daily air quality measurements. In such a scenario, temporal dependencies are typically short-range; thus, long-horizon forecasting (e.g., using the past 96 days to predict the next 96 days) is considered to be unrealistic. However, in our setup, a short-term prediction scheme is adopted (e.g., using air quality of the past 7 days and news reports released on the last day to predict air quality of the next day). Similarly, since SocialGood data tracks monthly unemployment rates, a more practical setting is to use a moderate-length historical window to predict the short-length future window (e.g. the past 14 months to predict the next 3 months), instead of a typical long-term setting (96 past months to predict future 96 months) that may not reflect real-world forecasting scenarios.

**Text Pairing.** TimeMMD’s original texts contain a significant number of missing values (NaNs) and are generally noisy or unstructured. Therefore, we decide to construct a synthetic multi-modal dataset based on the original time series. Synthetic news reports are generated based on two principles: (i) The generated news must not contain explicit

**Algorithm 4** ComputeMetrics( $x_{in}, x_{out}$ )

**Input:** Input and output windows  $x_{in}, x_{out}$ 
**Output:** A set of directional and fluctuation metrics

**A. Near-term Narrative:** Compare the mean of  $x_{out}$  with the tail of  $x_{in}$  to capture short-term level change.

**B. Severity:** Estimate a scale parameter  $\sigma$  from  $x_{in}$  using standard deviation, IQR, and MAD to ensure stability against outliers.

**C. Background Tendency:** Fit a linear slope to  $x_{in}$  and normalize by  $\sigma$  to obtain a trend score  $z_{past}$ , which determines direction and strength.

**D. Past-Window Variability:** Detrend  $x_{in}$  and compute residual volatility, smoothness ( $R^2$ ), and normalized mean absolute difference.

**E. (Future) Pattern Cue:** Fit a slope on  $x_{out}$ , normalize by  $\sigma$ , and record the resulting direction and magnitude.

**return** Metrics={A, B, C, D, E}

future labels or direct ground-truth information about the target variable. (ii) The content should include a mixture of accurate and inaccurate statements, thus mimicking the ambiguity, partial truth, and uncertainty commonly observed in real-world textual sources. To achieve this, we construct our own data using Algorithm 5. A qualitative comparison of the original and synthetic text is also provided in Figure 6.

Although the detailed prompt varies between datasets, they follow the same principle as summarized in Algorithm 5. We provide a prompt template C.2 to generate text.

**Example Prompt (Air-Quality Domain)**

You are an environmental journalist. Write one concise English bulletin ( $\sim 180$  words) about **recently observed** air-quality conditions over the past {n\\_days} days. Guidance (not a forecast):

- Near-term narrative: {narrative\_near}
- Severity: {severity\_near}
- Background tendency: {background}
- Past-window variability: {variability}
- Pattern cue: {pattern}

Rules: (1) Describe observed drivers only (e.g., inversions, wind, humidity, transport, anthropogenic sources); (2) No forecasts, numbers, or speculative language; (3) Keep factual, neutral, natural; one paragraph only.

**Algorithm 5** Synthetic Text Generation for TimeMMD

**Input:** Time series  $\{x_t\}_{t=1}^T$ ; input length  $L_{in}$ ; output length  $L_{out}$ ; stride  $s$ ; consistency probability  $p_c$ .

**Output:** Datasets  $\mathcal{D}_{train}, \mathcal{D}_{test}$  of  $(x_{in}, x_{out}, y_{text}, \text{consistency, metrics})$ 
**1. Slide:**

Initialize an empty list  $\mathcal{S}$  **for**  $i \leftarrow 1$  **to**  $T - (L_{in} + L_{out}) + 1$  **step**  $s$  **do**  
 $x_{in} \leftarrow [x_i, \dots, x_{i+L_{in}-1}]$ ;  
 $x_{out} \leftarrow [x_{i+L_{in}}, \dots, x_{i+L_{in}+L_{out}-1}]$ ;  
Append  $(x_{in}, x_{out})$  to  $\mathcal{S}$

**2. Split:**

Let  $N \leftarrow |\mathcal{S}|$ ,  $E \leftarrow \max(L_{in}, L_{out})$  Let  $c \leftarrow \lfloor 0.8N \rfloor$ ;  
 $\text{train\_idx} \leftarrow \{1, \dots, c\}$ ;  $\text{test\_idx} \leftarrow \{c + E, \dots, N\}$

**3) Generate:** **foreach**  $split \in \{\text{train, test}\}$  **do**

$\mathcal{D}_{split} \leftarrow []$ ; **foreach**  $j \in \text{idx}(split)$  **do**  
Metrics  $\leftarrow$  ComputeMetrics( $x_{in}, x_{out}$ );  
with prob.  $1 - p_c$  flip {past,near,future} and set  
consistency  $\in \{0, 1\}$   
LLM prompted generation ( $x_{in}$ , Metrics)  
Keyword Blocking: Filter predictive expressions  
from  $y_{text}$   
 $\mathcal{D}_{split}.\text{append}(x_{in}, x_{out}, y_{text}, \text{consistency, metrics})$

**return**  $\mathcal{D}_{train}, \mathcal{D}_{test}$ 

## D. More Discussion on MoME

### D.1. Other Theoretical Insights of MoE

The modern MoE architecture was originally introduced as a computationally efficient substitute for dense MLP layers in Transformers. Interestingly, beyond efficiency gains, subsequent studies observed that MoE-based models often achieve performance comparable to or even surpassing their dense counterparts (DeepSeek-AI et al., 2025), despite only activating a subset of parameters. We argue that this phenomenon is not accidental, but instead reflects a fundamental architectural difference between dense MLP and sparse MoE models. Over the years, many theoretical understandings of MoE have been established, but most of them focus on the perspective of latent clustering and token specialization (Chen et al., 2022; Kawata et al., 2025). In this paper, we provide a different theoretical insight of MoE from a geometric/denoising perspective, as detailed in Section 4.1.

### D.2. Discussions on Router Modulation

As described in Equation (5), auxiliary-modal signals can influence experts in two distinct stages: (i) Router modulation, which alters routing magnitudes and also changes which experts are selected; and (ii) EiLM modulation, which adjusts

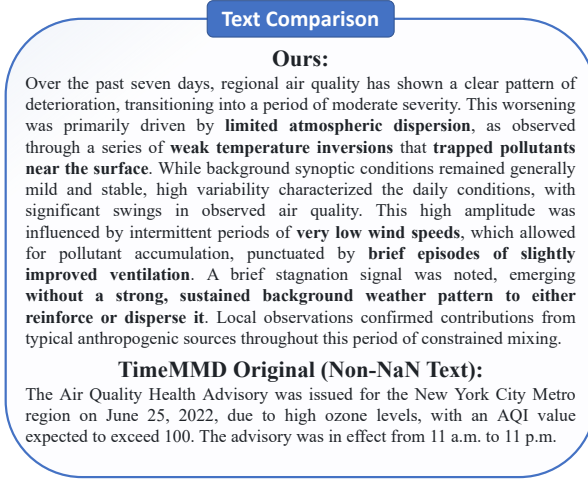


Figure 6. Textual information comparison between newly synthesized text and original data.

the behavior of experts already selected without affecting the selected Top- $K$  set. Although both mechanisms appear to modify the magnitude of the expert signal, their functions are fundamentally different. Router modulation reshapes the routing distribution and can completely change the Top- $K$  expert set, whereas EiLM only applies fine-grained adjustments within the already selected experts. As a result, router modulation has a much larger impact on model behavior. The downstream performance differences between these two mechanisms are evaluated in Section 5.5 and Table 10 in this Appendix section. We also examine how it affects the routing dynamics in Appendix F.

### D.3. Hyperparameter Sensitivity

Table 9 reports a comprehensive summary on how three critical hyperparameters in our design influence the downstream performance of the model. First, it is observed that a sparse activation of experts typically achieves better (or even optimal) performance than a full activation. This trend aligns with the theoretical insight of Theorem 4.2: sparse activation naturally performs a denoising effect by suppressing low-energy or noisy expert responses. Second, having context tokens generated from LLMs provides stable improvements over the uni-modal baselines. This observation further validates the effectiveness of incorporating multi-modal signals for time series prediction. Nevertheless, performance does not improve monotonically with an increase in the number of context tokens, and the best results are often achieved when a moderate number of context tokens (such as 3 to 4 tokens) are used. This result indicates that overly detailed semantic cues from LLM generation can increase the risk of overfitting, and ultimately harm generalization.

### D.4. Comparison of Fusion Strategies

To further validate the effectiveness of our proposed expert-modulation-based modality interaction, we compare it against several widely used fusion strategies in multi-modal time series models. Recent studies (Jin et al., 2024b; Zhang et al., 2025b) emphasize that token-level fusion plays a critical role in integrating textual and temporal information and examine various fusion strategies that substantially affect downstream performance. Based on the principles summarized in these studies, we implement five representative baselines that cover both the early-fusion and late-fusion paradigms. These baselines serve as comparison points for assessing whether expert-level modulation is a more robust paradigm than conventional token-fusion approaches.

The ablation models are as follows: (i) E1 [Early Fusion, Concatenation]: The time series token embeddings are first projected to the LLM’s hidden dimension, concatenated with the tokenized text, and then jointly fed into the LLM backbone; (ii) E2 [Early Fusion, Cross Attention]: Temporal token embeddings are attended to raw text tokens through a token-level cross attention, then the enhanced tokens are fed into the LLM backbone; (iii) L1 [Late Fusion, Additive]: The LLM processes the text independently, and its pooled embedding is projected and added to the output of the time series encoder before entering the downstream prediction head. (iv) L2 [Late Fusion, Concatenation]: It is similar to the L1 approach, except that it replaces addition by concatenation. (v) L3 [Late Fusion, Cross Attention]: Time series final embeddings are refined by cross attention over the LLM-derived text embeddings and then sent to the downstream head for prediction.

To ensure a fair comparison, all models use the same time series backbone, MoME (*w/o* EM), a uni-modal MLP-based MoE time series model without expert modulation. They also use the same LLM, Qwen-MoE, and Figure 2 also visualizes the architectures of the ablated models. The complete results for the comparative study are summarized in Table 11. Across the experiments, we evaluate not only downstream performance, but also training speed and memory consumption. Our proposed expert-modulation method, MoME, achieves the best on 7 of 8 tasks while offering significantly faster training per iteration. Notably, the memory consumption of our method is also small, which is comparable to simple fusion approaches (E1, L1, L2), and is substantially smaller than all cross attention based baselines (E2 and L3). Together, these results demonstrate that expert-modulation framework is an efficient and effective multi-modal integration mechanism, compared to classical token-fusion strategies.

# Experts	Activated	CT-1		CT-2		CT-3		CT-4		CT-5		CT-6		Avg_MAPE	Avg_MAE
		MAPE	MAE												
3	1	3.672	3.432	3.572	3.357	<b>3.685</b>	3.426	3.704	3.363	3.765	3.392	3.679	3.394	3.680	3.394
3	2	<b>3.621</b>	<b>3.299</b>	<b>3.530</b>	<b>3.243</b>	3.690	3.445	3.687	3.501	3.574	3.299	3.621	3.233	3.621	3.337
3	3	3.627	3.345	3.587	3.400	3.726	<b>3.379</b>	<b>3.489</b>	<b>3.309</b>	<b>3.515</b>	<b>3.259</b>	<b>3.513</b>	<b>3.194</b>	3.576	3.343
4	1	3.746	3.488	3.750	3.513	3.631	3.382	<b>3.632</b>	3.342	3.683	3.395	3.650	3.360	3.678	3.397
4	2	<b>3.461</b>	<b>3.139</b>	3.705	3.469	3.706	3.415	3.682	<b>3.338</b>	3.649	3.329	3.646	<b>3.290</b>	3.641	3.330
4	3	3.687	3.583	3.632	3.390	<b>3.561</b>	<b>3.242</b>	3.676	<b>3.338</b>	<b>3.572</b>	<b>3.331</b>	<b>3.601</b>	3.339	3.621	3.370
4	4	3.647	3.397	<b>3.563</b>	<b>3.229</b>	3.630	3.305	3.740	3.428	3.596	3.303	3.783	3.422	3.659	3.347
5	1	<b>3.572</b>	<b>3.325</b>	3.856	3.489	3.634	3.384	3.691	3.272	3.704	3.383	3.871	3.487	3.721	3.390
5	2	3.710	3.445	3.758	3.590	3.800	3.481	3.617	3.324	<b>3.584</b>	<b>3.290</b>	<b>3.556</b>	3.287	3.671	3.341
5	3	3.680	3.335	3.658	3.326	3.596	3.302	3.635	3.290	3.651	3.332	3.652	3.347	3.645	3.320
5	4	3.596	3.436	3.594	3.370	<b>3.477</b>	<b>3.174</b>	<b>3.594</b>	<b>3.266</b>	3.710	3.401	3.587	<b>3.231</b>	3.593	3.296
5	5	3.597	3.426	<b>3.531</b>	<b>3.300</b>	3.551	3.336	3.597	3.356	3.708	3.425	3.696	3.429	3.613	3.379
6	2	3.721	3.340	<b>3.627</b>	<b>3.316</b>	3.653	3.340	3.669	3.351	3.648	3.324	<b>3.596</b>	<b>3.288</b>	3.652	3.326
6	4	<b>3.559</b>	<b>3.293</b>	3.686	3.476	<b>3.611</b>	<b>3.249</b>	3.651	3.320	3.742	3.408	3.653	3.305	3.650	3.341
6	6	3.572	3.357	3.659	3.520	3.884	3.676	<b>3.504</b>	<b>3.182</b>	<b>3.596</b>	<b>3.291</b>	3.883	3.574	3.683	3.433
<b>Avg</b>		3.631	3.376	3.647	3.393	3.656	3.369	3.638	3.332	3.646	3.343	3.666	3.345		

Table 9. Ablation on how the number of experts, activated experts, and LLM-derived context tokens jointly influence proposed model performance. Here, the “CT- $k$ ” stands for  $k$  context tokens extracted by LLM, and the rows vary along two dimensions: the total number of experts in the MoE module (#Experts), and the number of experts activated by the Top- $K$  routing.

Task	Metric	MoME			Imp. (%)
		Base	w/ EiLM	w/ RM	
Environment	MAPE $\downarrow$	25.678	<b>15.434</b>	16.121	39.894
	MAE $\downarrow$	14.912	<b>8.317</b>	8.677	44.226
Energy	MSE $\downarrow$	0.018	<b>0.015</b>	0.017	16.667
	MAE $\downarrow$	0.086	<b>0.081</b>	0.084	5.814
Health (US)	MSE $\downarrow$	0.808	<b>0.379</b>	0.614	53.094
	MAE $\downarrow$	0.518	<b>0.359</b>	0.429	30.695
Health (AFR)	MSE $\downarrow$	0.125	0.116	<b>0.103</b>	17.600
	MAE $\downarrow$	2.318	2.414	<b>2.303</b>	0.647
Social Good	MSE $\downarrow$	1.743	<b>1.419</b>	1.455	18.589
	MAE $\downarrow$	0.487	<b>0.417</b>	0.429	14.374

Table 10. Ablation on TimeMMD. Imp. (%) is computed by comparing the best variant against the w/o EiLM setting. For Health (AFR), metrics are reported in units of  $10^2$ .

## D.5. Training Efficiency

Figure 7 compares the convergence behavior of different models tested in the MT-Finance dataset. MoME and MMLinear exhibit substantially faster training convergence than both iTransformer and TimeMoE. When removing expert modulation components (i.e., removing EiLM, RM module), the two uni-modal variants, MoME (w/o EM) and MMLinear (w/o EM) consistently slow convergence and lead to higher final training loss. These results suggest that expert modulation not only improves predictive accuracy, but also accelerates optimization, making the training process even more efficient. Additionally, we observe that most baseline models converge within the first 10 epochs, whereas the proposed MoME model continues to improve beyond this point. This indicates that MoME possesses greater representational capacity and is able to extract increasingly useful signals from the multi-modal data, suggesting stronger model expressivity compared to conventional architectures.

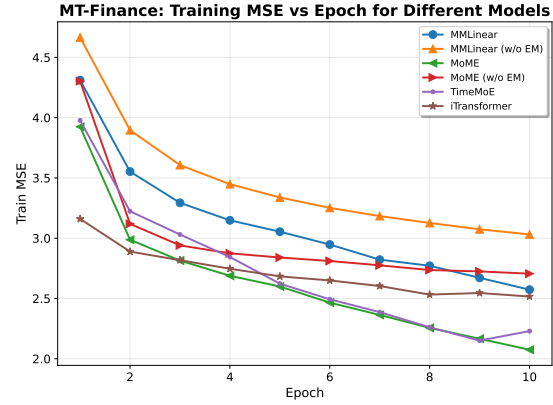


Figure 7. Comparison for training efficiency on two benchmarks.

## D.6. Hyperparameter Setting for Main Experiments

Table 12 summarizes the key hyperparameter configurations used in all main experiments. For a fair comparison, identical settings are applied to all models, unless explicitly stated otherwise. In the experiments, we also implemented several token-level fusion baselines, including MLP (MoE)+LM, Time-MoE+LM, DLinearP+LM, and all fusion variants reported in Table 11. For all of these models, the LLM is finetuned using LoRA (Hu et al., 2022) to ensure parameter-efficient adaptation. Specifically, LoRA updates are only applied to attention projection layers  $[q_{proj}, k_{proj}, v_{proj}, o_{proj}]$ .

## E. Case Study: How Text Helps?

Although Table 5 and Table 6 demonstrate the performance gains from multi-modality data and the expert-modulation

Model \ Metric	MT-Finance						SocialGood					
	Time (s/iter)		Space (M)		Performance		Time (s/iter)		Space (M)		Performance	
	Train	Inference	TS-Encoder	Instr/Align	3-Acc	5-Acc	Train	Inference	TS-Encoder	Instr/Align	MSE	MAE
<b>Uni-Modal Baseline</b>												
MoME( <i>w/o</i> EiLM)	0.01	0.01-	0.0095	\	46.233	40.411	0.01-	0.01-	0.0095	\	1.743	0.487
<b>Expert Modulation</b>												
MoME( <i>w/</i> EiLM)	0.47	0.46	0.0126	0.0700	<b>60.616</b>	<b>51.027</b>	0.38	0.36	0.0126	0.0700	<b>1.419</b>	<b>0.417</b>
MoME( <i>w/</i> RM)	0.47	0.47	0.0127	0.0700	<b>62.671</b>	<b>47.945</b>	0.38	0.36	0.0127	0.0700	<b>1.455</b>	<b>0.429</b>
<b>Token Alignment</b>												
MoME( <i>w/o</i> EiLM)+E1	1.19	0.47	0.0095	0.0676	<b>48.288</b>	33.219	1.03	0.37	0.0095	0.0676	1.908	0.730
MoME( <i>w/o</i> EiLM)+E2	1.25	0.47	0.0095	16.853	<b>47.603</b>	<b>41.096</b>	1.05	0.37	0.0095	16.853	<b>1.504</b>	0.534
MoME( <i>w/o</i> EiLM)+L1	1.19	0.47	0.0095	0.0676	<b>63.013</b>	<b>51.027</b>	1.03	0.36	0.0095	0.0676	2.125	0.620
MoME( <i>w/o</i> EiLM)+L2	1.21	0.47	0.0095	0.0676	<b>62.329</b>	<b>47.603</b>	1.03	0.37	0.0095	0.0676	<b>1.699</b>	0.553
MoME( <i>w/o</i> EiLM)+L3	1.58	0.47	0.0095	16.853	<b>49.315</b>	<b>41.781</b>	0.49	0.37	0.0095	16.853	1.869	0.525
Model \ Metric	MT-Weather						Health-US					
	Time (s/iter)		Space (M)		Performance		Time (s/iter)		Space (M)		Performance	
	Train	Inference	TS-Encoder	Instr/Align	P-Acc	F-Acc	Train	Inference	TS-Encoder	Instr/Align	MSE	MAE
<b>Uni-Modal Baseline</b>												
MoME( <i>w/o</i> EiLM)	0.01-	0.01-	0.0095	\	87.534	49.594	0.01-	0.01-	0.0095	\	0.808	0.518
<b>Expert Modulation</b>												
MoME( <i>w/</i> EiLM)	0.49	0.47	0.0126	0.0700	<b>93.496</b>	<b>52.575</b>	0.37	0.36	0.0126	0.0700	<b>0.379</b>	<b>0.359</b>
MoME( <i>w/</i> RM)	0.49	0.48	0.0127	0.0700	92.141	50.136	0.37	0.36	0.0127	0.0700	0.614	0.429
<b>Token Alignment</b>												
MoME( <i>w/o</i> EiLM)+E1	1.22	0.48	0.0095	0.0676	86.450	41.192	1.04	0.37	0.0095	0.0676	<b>0.802</b>	<b>0.489</b>
MoME( <i>w/o</i> EiLM)+E2	1.27	0.48	0.0095	16.853	<b>87.805</b>	<b>49.594</b>	1.05	0.38	0.0095	16.853	<b>0.772</b>	0.562
MoME( <i>w/o</i> EiLM)+L1	1.21	0.47	0.0095	0.0676	64.228	38.482	1.05	0.37	0.0095	0.0676	1.694	0.872
MoME( <i>w/o</i> EiLM)+L2	1.22	0.48	0.0095	0.0676	63.415	44.986	1.05	0.38	0.0095	0.0676	1.022	0.693
MoME( <i>w/o</i> EiLM)+L3	1.61	0.47	0.0095	16.853	<b>90.515</b>	42.818	0.51	0.38	0.0095	16.853	1.088	0.663

Table 11. Comparison with token-fusion strategies. E1–E2 denote early-fusion methods, and L1–L3 denote late-fusion methods. For example, MoME (*w/o* EM) + E1 indicates an early token-fusion variant that injects textual information by token concatenation.

Category	Setting
<b>TS-Encoder</b>	Layers = 3; Hidden dim = 32; Dropout = 0.1; Number of Heads = 4; Patch Length = 8
<b>EiLM</b>	Experts = 4; Top- <i>K</i> = 2; Instructor query = 3; Router Modulation = Enabled/Disabled; Modulation = Enabled/Disabled
<b>LLM Encoder</b>	LLM Hidden Dimension = 2048 Max Text Length = 2048

Table 12. Hyperparameter configuration for main experiments.

framework, these numbers alone do not reveal how textual information actually contributes to prediction. Second, it remains unclear whether the improvements stem merely from the expressive power of the LLM, or whether the model truly “understands or comprehends” the news content. Finally, real-world text is often imperfect or even inconsistent with future outcomes; for example, financial reports can contain conflicting assessments or incorrect projections about the prospects of a company. Understanding how MoME behaves under such ambiguous or unreliable textual input is therefore essential. To provide a deeper understanding, we conduct case studies in strong baselines and ablated variants.

**Successful Cases.** Figures 9 and 10 present two examples in which financial reports are correct about subsequent market behavior. In Figure 9, the report sends several negative signals, including a “surprising negative earnings

warning” and a “clear recommendation to sell the stock”. In this scenario, both proposed model families, [MoME (*w/o* EM), MoME (*w/* EiLM), MoME (*w/* RM)] and [MMLinear(*w/o* EM), MMLinear, MMLinear(*w/* RM)]], show clear improvements when expert modulation or router modulation is activated. Crucially, the uni-modal MoE variants [MoME(*w/o* EM) and MMLinear(*w/o* EM)] incorrectly predict an upward future trend. Once expert modulation is enabled, however, the predicted trajectory reverses: both models correctly forecast a downward trend, which is consistent with the negative sentiment in the report. This demonstrates that activation of expert modulation does not merely refine the output but can fundamentally alter the predicted trend evolution. Meanwhile, early-fusion models, such as MLP (MoE)+LM and TimeMoE+LM fail to produce the correct downward prediction, where they still forecast a positive or weakly increasing trend. This contrast highlights that using simple early fusion strategies to connect time series model and LLM has fundamental limitations.

Figure 10 provides another successful example. This report acknowledges a recent upward revision in the stock price, but ultimately concludes that the stock is expected to remain neutral in the near-term future. This subtle combination of short-term momentum and medium-term stabilization poses a significant challenge for uni-modal time series models. In contrast, our expert-modulation models, MoME (*w/* EiLM) and MoME (*w/* RM), predict a nearly flat and stable trajectory, closely matching the interpretation of the report.

Together, these case studies demonstrate that our proposed modality interaction framework enables the model to effectively integrate information across modalities, producing forecasts that reflect the semantic signals embedded in both the textual reports and the time series patterns.

**Struggling Cases.** Figure 11 illustrates a clear failure case. The corresponding report expresses an overwhelmingly positive outlook for the stock, using phrases such as “the company’s earnings outlook appears to be robust” and indicating expectations that the firm will “continue to outperform the broader market in the near term.” In this scenario, both uni-modal and multi-modal models consistently predict a rising trend, particularly, no model successfully resists the misleading reports information. Nevertheless, we note that MoME and MMLinear still outperform their uni-modal ablations, in terms of evaluation metric, indicating that our proposed method remains safe to use because its performance does not catastrophically degrade even when cross-modal information is inconsistent.

Figure 12 presents another scenario in which the associated financial report conveys mixed signals: it cautiously recommends holding the stock while simultaneously highlighting a compelling growth outlook. Such contradictory cues also lead to uncertainty in model predictions. Within the group [MoME (*w/o* EM), MoME (*w/* EiLM), MoME (*w/* RM)], we observe that the option of expert modulation has a minimal effect, where both the trend and quantitative metrics remain largely unchanged. However, in the [MMLinear (*w/o* EM), MMLinear (*w/* EiLM), MMLinear (*w/* RM)] group, expert modulation drastically alters the behavior of the model: without modulation, the model produces an almost flat forecast, while with expert modulation, it clearly predicts an upward trend. This contrast suggests that, under the multi-modal learning framework, the model is indeed leveraging textual information rather than relying only on the expressive capacity of LLM. Nevertheless, when the text itself is ambiguous or contradictory, the model may still fail to form reliable forecasts.

## F. Dynamics of Token Routing

In Section 5.5, we briefly discuss that MoE tends to route similar tokens to similar subsets of experts. To further clarify this behavior, we first specify what constitutes a token in time series. Existing architectures predominantly adopt two tokenization schemes: (i) treating each temporal patch as a token (Nie et al., 2023), or (ii) treating each entire time series channel as a token (Liu et al., 2024b). Under these formulations, token similarity in time series may arise from different factors. Based on our observations, similarity between temporal tokens can be attributed to two aspects: morphological patterns (i.e., the shape of local temporal

dynamics) and magnitudes (i.e., overall signal scale).

**Morphological Pattern based Selection.** In this experiment, we treat channels as tokens and visualize the routing behavior of MoE-based time series model on the ETTm2 dataset (Figure 5 (b)). The temporal shapes of Channels 0-3 are very similar, while Channels 4 and 5 exhibit distinctly different patterns, and Channel 6 resembles a smoothed version of the first group. Similarly, the router assigns Channels 4 and 5 predominantly to Expert 1, whereas the remaining channels strongly prefer Expert 2. In general, we find that channels with similar temporal dynamics, including local trends and fluctuation patterns, tend to activate similar subsets of experts. This suggests that the router tends to learn a morphological pattern based grouping, assigning experts to families of temporal shapes.

**Magnitude-based Selection.** In this experiment, we treat short temporal patches as tokens and test routing dynamics on the MT-Finance dataset. A different form of specialization is observed (Figure 8), where patches of similar magnitude tend to be routed to the same experts. Such a scale-based specialization is particularly useful in domains where individual time series samples differ significantly in their value ranges. For example, stock prices (MT-Finance) of different companies can vary significantly by magnitude.

The right panel of Figure 8 further visualizes the effect of activating router modulation in expert modulation (i.e., the MoME (*w/* RM) variant). Although activating RM improves performance in several experiments (Table 5), it tends to lead to expert collapse, where the router concentrates most tokens onto a small subset of experts.

**Reflection on Load-Balancing.** Conventional MoE implementations often introduce load-balancing loss to prevent expert collapse and encourage “uniform” expert utilization. However, our empirical comparison between MoME and MoME (*w/* RM) indicates that uniform routing can also suppress meaningful expert specialization. In particular, time series tokens naturally differ in both temporal patterns and signal magnitudes, and forcing them to be evenly distributed across experts may disrupt the router’s ability to form coherent clusters that reflect these intrinsic differences.

These observations suggest that effective routing in time series MoE models requires a more nuanced trade-off between expert uniformity and specialization, rather than enforcing strict load balancing. Similar conclusions have also been reported in recent studies (Guo et al., 2026).

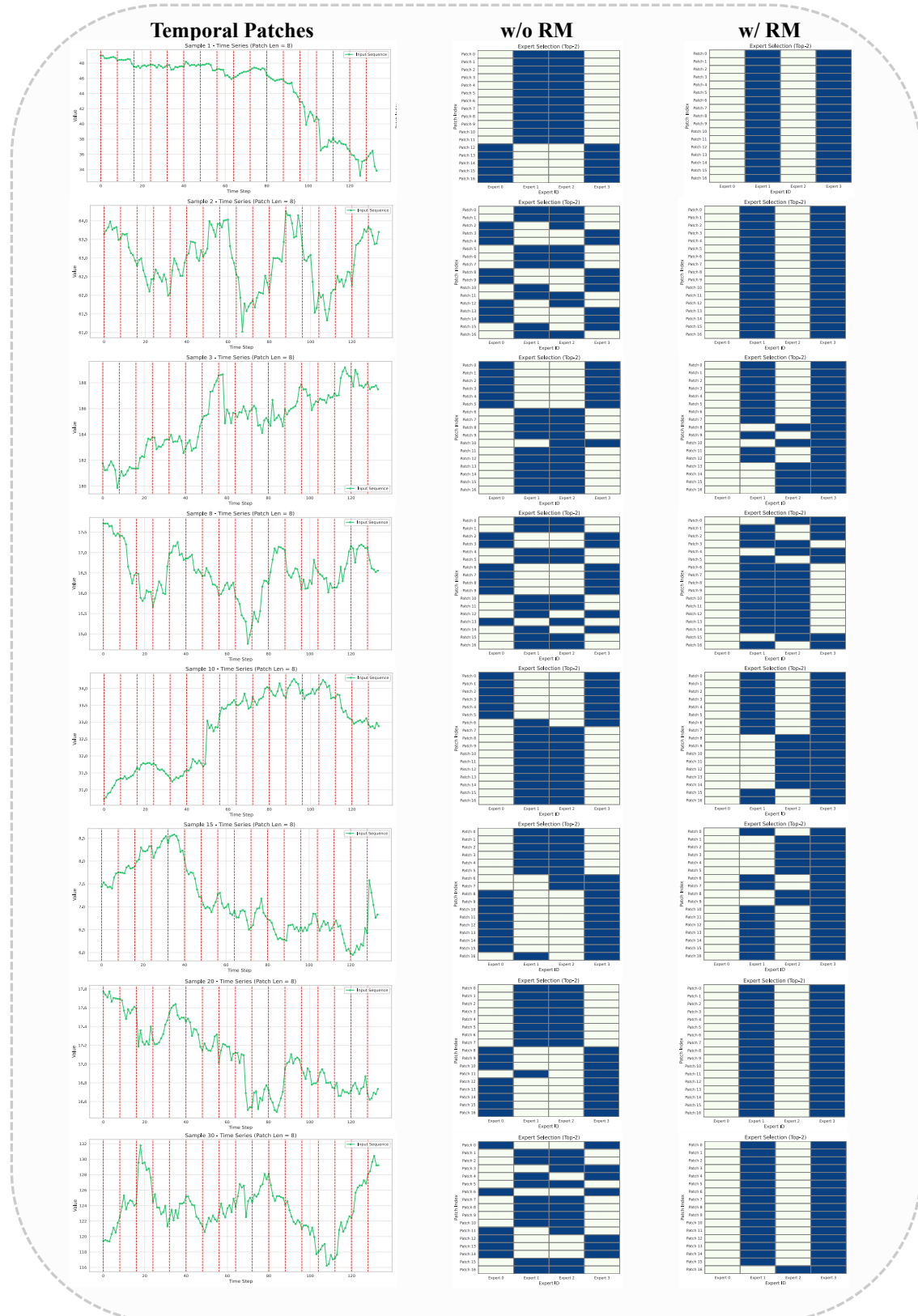


Figure 8. The dynamic of routing when router modulation activated.

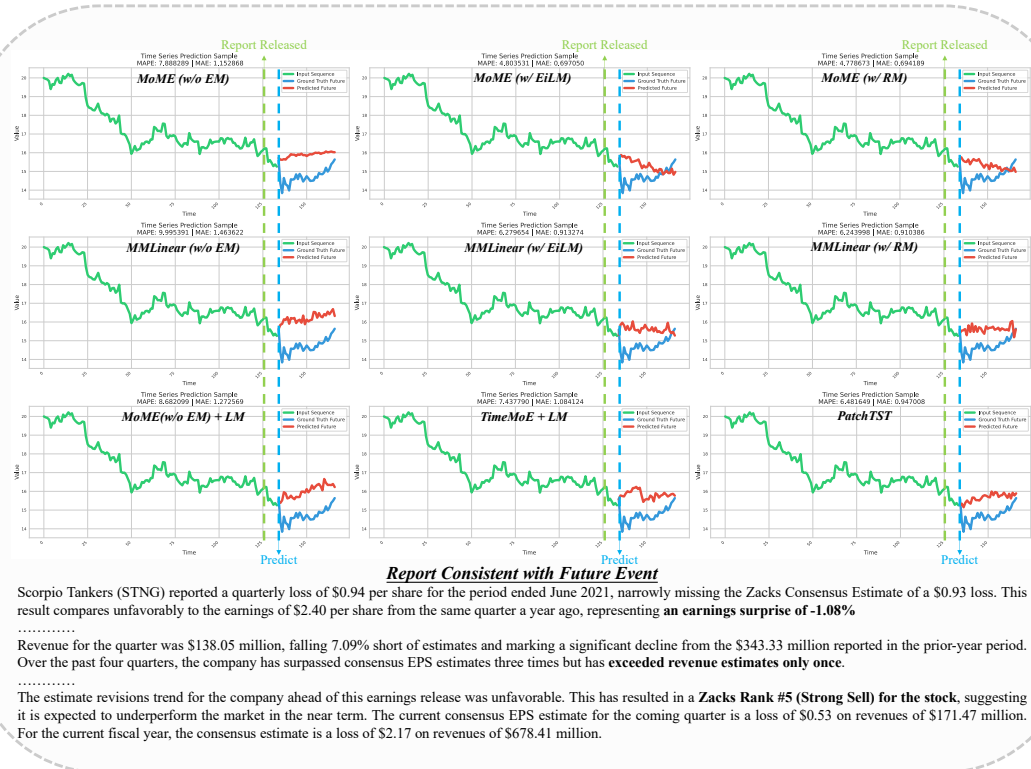


Figure 9. Stock price forecasting(1): when news report are consistent with actual future state.

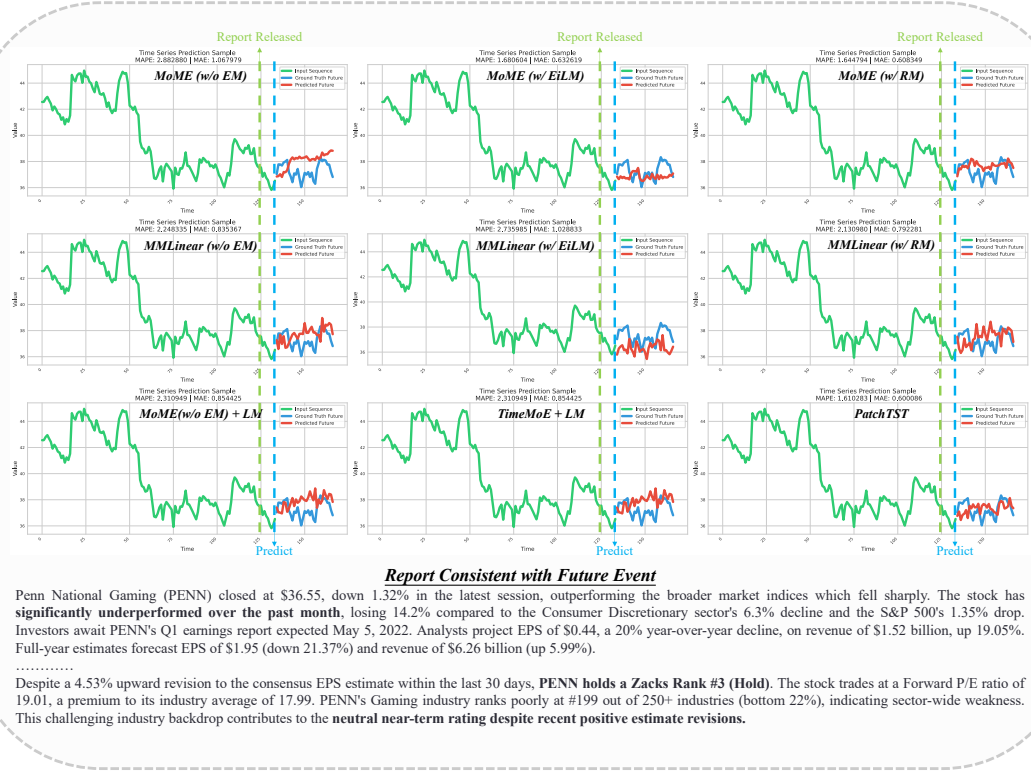
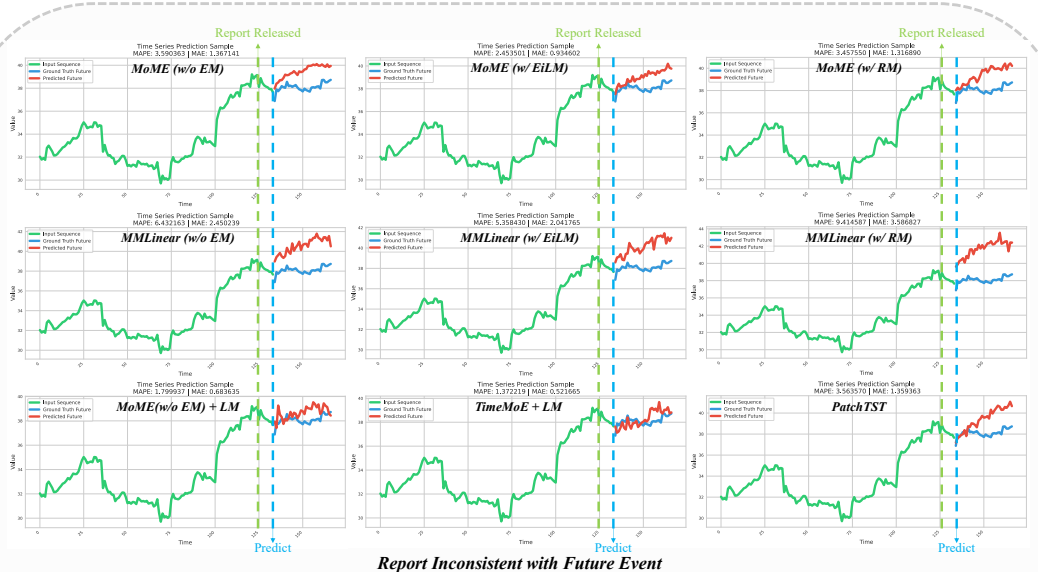


Figure 10. Stock price forecasting(2): when news report are consistent with actual future state.

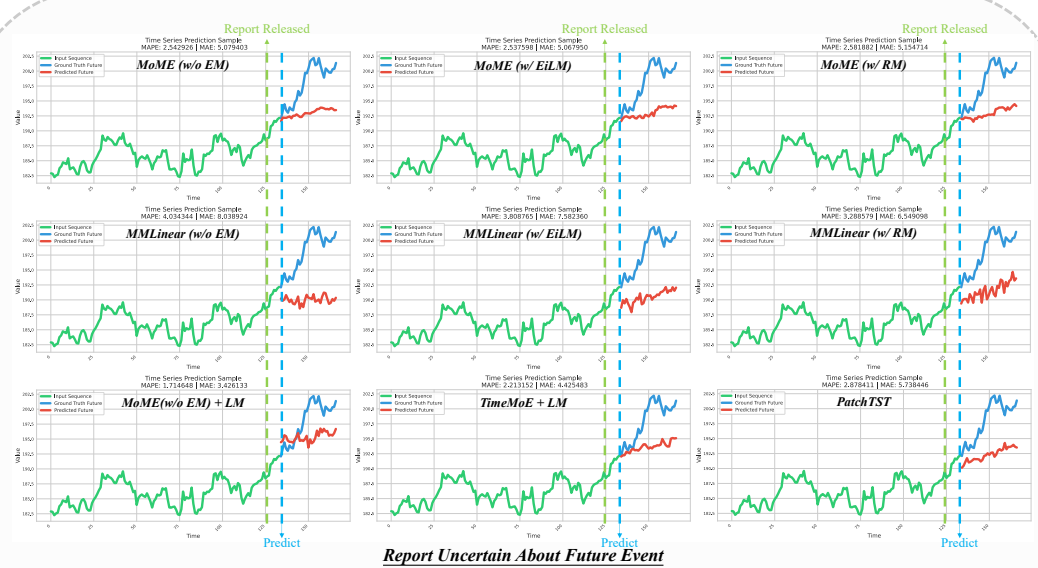


STMicroelectronics (STM) has demonstrated strong market performance, returning +18.8% over the past month compared to the Zacks S&P 500 composite's +10.6% gain. The stock's **momentum exceeds** both the broader market and its industry peers, as the Zacks Semiconductor - General industry has gained 29.8% over the same period.

The company's **earnings outlook appears robust**, with significant estimate revisions across all time frames. For the current quarter, STMicroelectronics is expected to post earnings of \$1.13 per share, representing a year-over-year increase of +37.8%. The Zacks Consensus Estimate for this quarter has been revised upward by +2.1% over the last 30 days. For the current fiscal year, the consensus earnings estimate of \$4 reflects a substantial +85.2% year-over-year growth, with this estimate rising +3.3%...

The combination of strong earnings estimate revisions and solid valuation metrics has earned STMicroelectronics a **Zacks Rank #2 (Buy)**. The stock also carries a **Value Style Score of A**, indicating it trades at a **discount to its peers**. These factors suggest the stock may **continue to outperform** the broader market in the near term.

Figure 11. Stock price forecasting(3): when news report are inconsistent with actual future state.



Jack Henry & Associates (JKHY) currently holds a **Zacks Rank #3 (Hold)** but demonstrates **compelling growth characteristics**. The company has achieved a **Growth Style Score of A**, with projected year-over-year earnings growth of 1% for the current fiscal year. This **positive outlook** is supported by recent analyst confidence, as one analyst raised their fiscal 2023 estimate in the last 60 days, boosting the Zacks Consensus Estimate by \$0.01 to \$4.99 per share.

The company **maintains a strong track record of exceeding expectations**, boasting an average earnings surprise of 8.6%. This history of outperformance complements its solid **VGM Score of B**, which reflects favorable **combined value, growth, and momentum characteristics**.

Despite the Hold rating, these fundamental strengths present a **compelling case for investor consideration**. The stock's combination of upward earnings revisions, **strong growth metrics**, and consistent historical performance suggests underlying strength that may not be fully captured by its current rank.

Figure 12. Stock price forecasting(4): when news report are uncertain about actual future state.